Modelling SCR Installation

by

Stephanie Mennecier (PET)

Fourth-year undergraduate project

In Group D, 2014/2015

I hereby declare that, except where specifically indicated, the work submitted herein is my own original work

Signed …………………………………………………………………………………… Date ………………………………

Table of Contents

1 Technical Abstract

Fatigue stresses associated with extreme storms, vessel movements and vortex-induced vibrations are critical to steel catenary riser (SCR) performance. The critical location for fatigue damage is in the touchdown zone (TDZ); the region where cyclic interaction between the riser and seabed occurs. As seafloor stiffness cannot be estimated with a great deal of reliability, neither can the bending stresses and fatigue life of the risers.

Aubeny and Biscontin (2006) proposed a non-linear load-displacement (P, y) model to describe seafloor-riser interaction based on model testing. It considers the problem in terms of a linearly elastic pipe resting on a bed of uncoupled non-linear springs and requires the iterative solution of a fourth-order ordinary differential equation for the differential displacement along the pipe, Δy. The load-displacement model can take account of non-linear soil behaviour, suction and breakaway, yielding, and soil degradation under cyclic loading. It requires a number of input parameters related to riser and soil properties.

One of the most critical loading scenarios within the TDZ occurs during installation. Three additional model parameters are required to simulate it: the installation angle θ and the two locations along the riser between which the installation loading will be applied, x_1 and x_2. Installation loading is modelled by applying a rotation θ at the node x_2 m along the riser and determining the resultant deflected shape of the riser before updating all the state variables. To simulate that the soil to the side of the rotation where the riser has been vertically displaced remains untouched, the soil surface profile is reset to the riser's self-weight penetration depth. The rotation is then released and this process is repeated at each node in turn between x_1 and x_2 until a full post-installation soil surface profile has been calculated.

Calibrating the model with field observations by Bridge and Willis (2002) and Bridge and Howells (2007) allowed a realistic value of θ = 0.09 radians to be estimated. Further simulations demonstrated that increasing the value of θ has the effect of increasing the post-installation trench depth and moment envelopes of the riser during installation and subsequent operational loading. This is because the shear strength profile of the soil, and

hence its resistance, increases with trench depth, inducing greater moments in the riser. Consequently, this has a detrimental impact on the riser's fatigue life and indicates that current predictions neglecting installation loading may not be conservative.

A parametric study looking at the effect of the riser's diameter and penetration rate on trench depth and bending moments identified that increasing the riser's diameter has a negative effect on its fatigue life; however, increasing the penetration rate served to reduce the maximum moments experienced by it and its working life. Despite the model being quasi-static, the effect of penetration rate could be analysed by calibrating the degradation model parameters with two large-scale NGI tested carried out at differing penetration rates. On account of the observations drawn from the study, it is recommended that when installing offshore risers, the installation angle is kept as shallow as possible and the riser diameter is kept to a minimum to reduce moments both during installation and the working life of the riser and increase the riser's fatigue life.

In conclusion, installation has been shown to be one of the most critical loading scenarios during the life of a SCR and modelling this scenario has enabled more realistic bending moment and trench depth predictions along the riser which allows for improved fatigue life estimates.

2 Introduction

As oil and gas production moves into deeper and deeper waters, new designs for riser pipes have had to be developed. These pipes are used to transport oil from the well head on the seafloor to the offshore floating structure. One of the most popular systems is the steel catenary riser (SCR) system which was first used by Shell in 1994 (Mekha, 2001). The risers are typically 0.2 - 0.35 *m* in diameter and operate at a pressure of 13.5 - 41.5 *MPa* (Howells, 1998).

Fatigue stresses associated with extreme storms, vessel movements and vortex-induced vibrations are critical to SCR performance. The critical location for fatigue damage is in the touchdown zone (TDZ); the region where cyclic interaction between the riser and seabed occurs. The maximum bending stresses also typically occur in this section of the riser. They are very are sensitive to seafloor stiffness such that an SCR will experience greater bending stresses on rigid soil than on soft soil. At present, seafloor stiffness cannot be estimated with a great deal of reliability and hence neither can the bending stresses and fatigue life of the risers.

Despite linear elastic seafloor models providing useful insights (Pesce, et al., 1998), full scale model tests (Bridge, 2002; Bridge 2004) have shown that the riser problem involves complex nonlinear processes including:

- Trench formation
- Non-linear soil stiffness
- Finite soil suction
- Breakaway of riser from the seafloor

In addition, studies indicate that soil stiffness degradation effects can be significant when dealing with cyclic loading of pipes on soil (Dunlap, 1990; Clukey, 2005) such as those experienced by the riser in the TDZ.

In order to try and understand this behaviour further, Aubeny and Biscontin (2009) developed a non-linear seafloor-riser interaction model in MATLAB which considers the problem in terms of a linear elastic pipe resting on a bed of springs whose stiffness' are described by non-linear load displacement (P-y) curves. The problem is treated as quasi-static, disregarding the inertia of the riser, and requires the iterative solution of a fourth order ordinary differential equation by means of the finite difference method. The initial version of the model allowed for virgin penetration, non-linear soil stiffness, soil suction and breakaway however it did not take into consideration soil degradation. The model has since been developed by You (2012) so that accumulated deflection during the loading of the soil serves as a measure of energy dissipation in order to quantify soil degradation. Any combination of imposed vertical displacements, tension and moments can be applied at one end of the riser however, lateral motions of the riser have been neglected to simplify the analysis (despite evidence that they can affect riser performance (Morris, 1988; Hale, 1992)), by assuming that they are less than 4 pipe diameters wide. This assumption also justifies the use of small-strain, small-deflection beam theory.

Further improvements to the model, detailed in this report, involve the incorporation of modelling riser installation. The motivation being that one of the most critical loading scenarios occurs when the riser is installed, during which it undergoes large deformations creating trenches several diameters deep (Bridge & Howels, 2007). The effect of these deep post-installation trenches on the riser's fatigue life is currently under dispute with some authors reporting an decrease in fatigue damage due to trench formation (Bhat, et al., 2013 ; Giertsen, et al., 2004) while other suggest that is detrimental to the fatigue life of the SCR (Clukey, et al., 2007 ; Nakhaee & Zhang, 2008) . The current MATLAB model does not take into account the installation process at all but rather assumes that the initial trench depth before operational loading is applied is solely due to the self-weight of the riser. Therefore modify the model to include the installation process will allow for more accurate predictions of the bending moments the riser is subject to and its fatigue life.

3 Background Theory

3.1 Touchdown Zone

The SCR can be divided into three regions as shown in Figure 1 (Bridge, 2005):

- *Catenary zone* - the riser hangs in a catenary shape
- *Buried zone* - the riser is in a trench formed by the riser interaction with the seabed
- *Surface zone* - the riser rests statically on the seafloor.

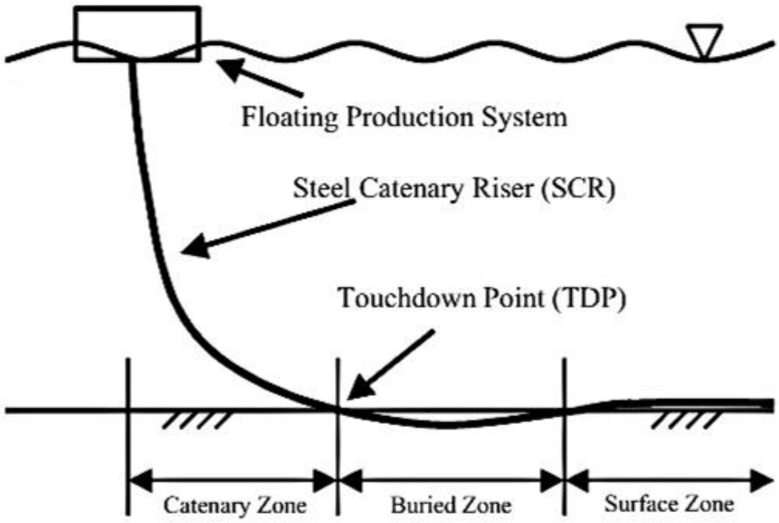

Figure 1 General Catenary Arrangement (Bridge, 2005)

The touchdown zone (TDZ) is the region where cyclic interaction between the SCR and seabed takes place and it consists mainly of the buried zone, along with small sections of the catenary and surface zones. The touchdown point (TDP) is continually moving along the length of the riser due to the loading applied to it and these motions cause the SCR to dig itself into a trench. The trench near the TDP is wide and shallow but towards the mid-point of the buried zone, the riser motions form a deeper, narrower trench (Bridge & Howels, 2007). The mechanics of trench formation are not well understood however it is thought that the dynamic motions of the riser, along with scour, sediment transport and seabed currents produce the trench.

3.2 Loading on an SCR

3.2.1 Installation

There are two main loading scenarios that an SCR is subject to during its lifetime. The first is installation. There are two common methods of installing SCRs: the J-lay and S-lay methods, so named due to the shape of the pipe during installation (Figure 2). The S-lay method is used in shallow waters whereas the J-lay method is more suitable for deep water installations where the water depth ranges between 400 - 1500 *m*. The reason for this is because, if used in shallow waters, the J-lay method would require a departure angle near to the horizontal in order for the pipe to fall in a catenary shape to the seabed. Rather, the optimum angle of departure for the J-lay method is typically between 4 and 15 degrees to the vertical (2H Offshore Engineering Ltd., 2006).

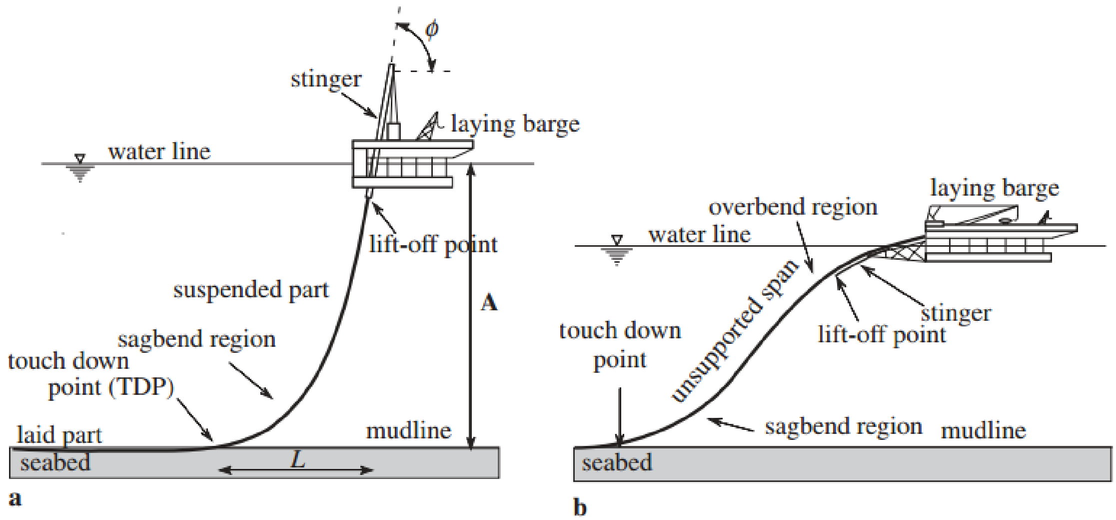

Figure 2 Deployment of marine pipelines by (a) the J-lay, and (b) the S-lay methods (Callegari & Lenci, 2005)

Some of the advantages and disadvantages of the J-lay technique over the S-lay are discussed below (Callegari, 2005 ; Pulici, 2003 ; 2H Offshore Engineering Ltd., 2006).

Advantages:

- Riser laid in a more natural configuration which allows for stresses to be kept well within the linear elastic limit.

- Reduction of the horizontal distance between the vessel and the touchdown point which enables better positioning of the pipe – up to 1m accuracy.
- Reduction of the horizontal force applied to the end of the riser by the vessel engines, hence a lower lay tension.
- Elimination of the section of the riser near the barge with high curvature which can produce residual stresses.
- Less susceptible to weather conditions.

Disadvantages:

- Processing operations are more difficult along a steep ramp.
- There is only space for a single joining station which can lead to slower laying rates.
- Bigger vessels with more power are needed for dynamical positioning under all operating conditions.
- More expensive.
- Good quality offshore welds are required in order to achieve sufficient fatigue lives.

3.2.2 Working Life Loading

The second loading scenario occurs during the SCR's operating life when it typically hangs from a floating oil platform and as such is subject to wave, current and wind loading. It connects to the platform via either a flex joint or taper stress joint which transfer the dynamic motions of the oil platform directly to the top of the SCR and cause the touchdown point (TDP) to move along it. The main forms of dynamic motion are (Bridge, 2005):

- *First order motions* – frequency motions caused by wave action on the platform
- *Second order motions* – low frequency motions caused by swell waves and light winds. Also known as slow drift motions
- *Static offset* – displacement resulting from mean environmental loads such as currents, waves and winds or system failures such as failed mooring lines

These motions result in cyclic loading on the seabed causing the riser to penetrate further into the soil. This in-contact cycling of buried pipelines, where the pipeline does not lose contact with the soil, has been written about by many authors including Dunlap et al. (1990). They show that cyclic motion softens the seabed causing the soil stiffness to reduce as the number of cycles increases.

3.3 Overview of Modelling the Installation Process

In their 2006 paper Aubeny and Biscontin proposed a non-linear load-displacement (P, y) model to describe seafloor-riser interaction inferred from model testing. It considers the problem in terms of a linearly elastic pipe resting on a bed of uncoupled non-linear springs (Figure 3) and requires the iterative solution of a fourth-order ordinary differential equation for the differential displacement along the pipe Δy.

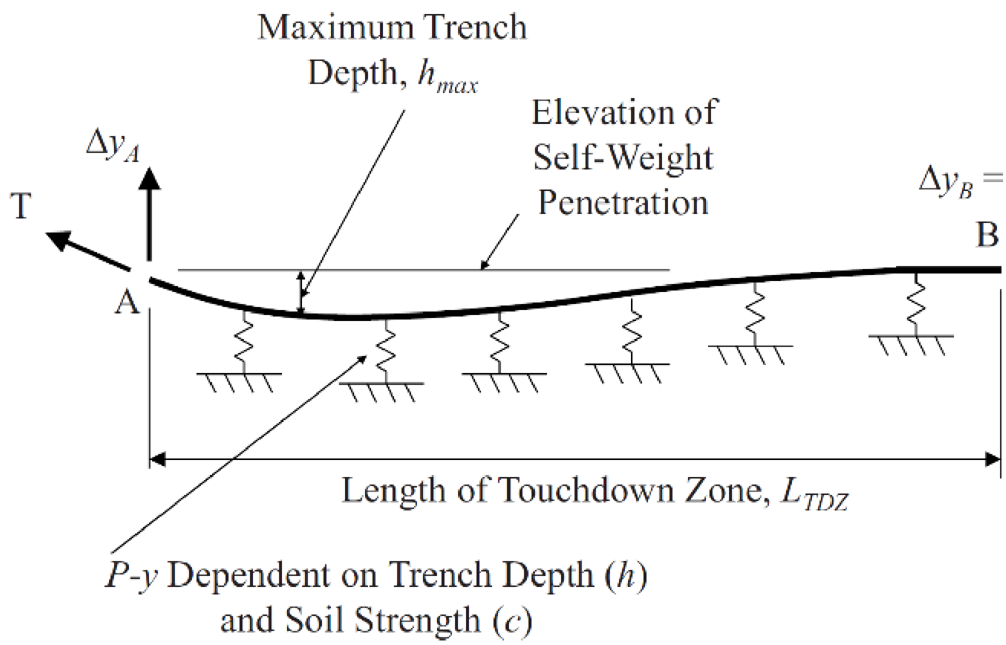

Figure 3 Spring-Pipe Model (Aubeny & Biscontin, 2006)

When simulating the installation of the riser, this seafloor-riser interaction model and the solution of the governing differential equation are manipulated to determine the soil surface profile after installation and its moment envelope during the procedure. The overall process to achieve this is outlined in flow chart in Figure 4.

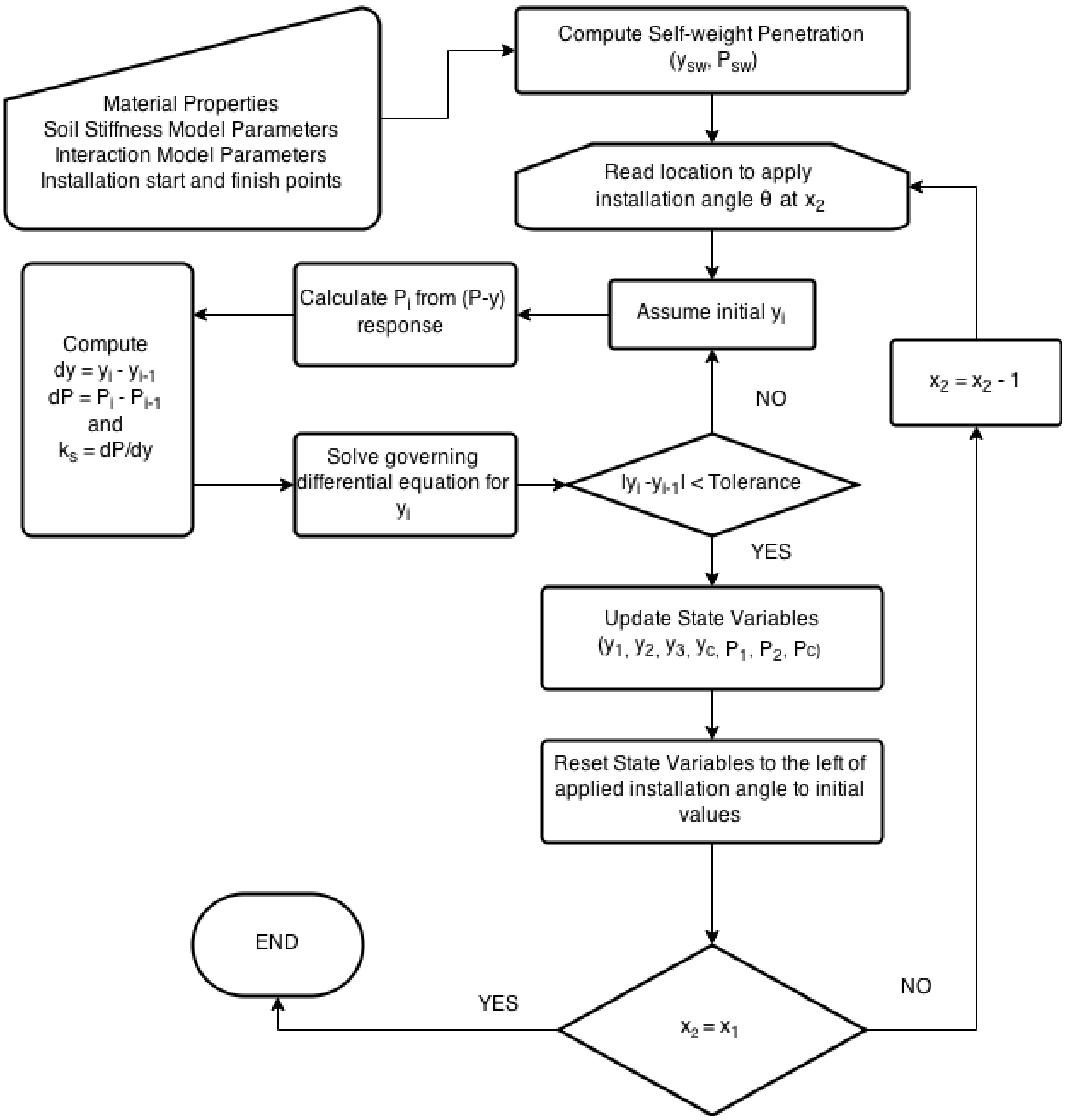

Figure 4 Flowchart outlining modelling of SCR installation process

Firstly the soil and riser parameters are manually input along with three specific installation parameters; the installation angle θ, and the two locations along the riser between which installation will be simulated, x_1 and x_2 (Figure 5). The self-weight penetration of the riser is computed and acts as the baseline trench depth. Then a rotation, θ, is applied at the node x_2 m along the riser and the resultant deflected shape is assumed. This shape is then used to calculate the soil resistance P for each nodal spring and hence its secant stiffness k_s. Having estimated k_s at each node, the governing differential equation for the riser can be solved iteratively with appropriate boundary conditions by applying the central difference method to calculate the true deflected shape before updating the state variables.

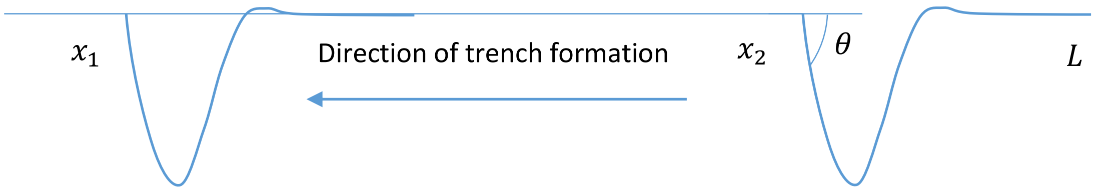

Figure 5 Installation parameters

An example of the deflected shape of a 80m riser which has had a rotation applied to it at 50m along it length is shown in Figure 6. The trench depth to the left of where the rotation was applied is then reset to the riser's self-weight penetration (Figure 7) as during the real installation process this soil would not have yet been disturbed.

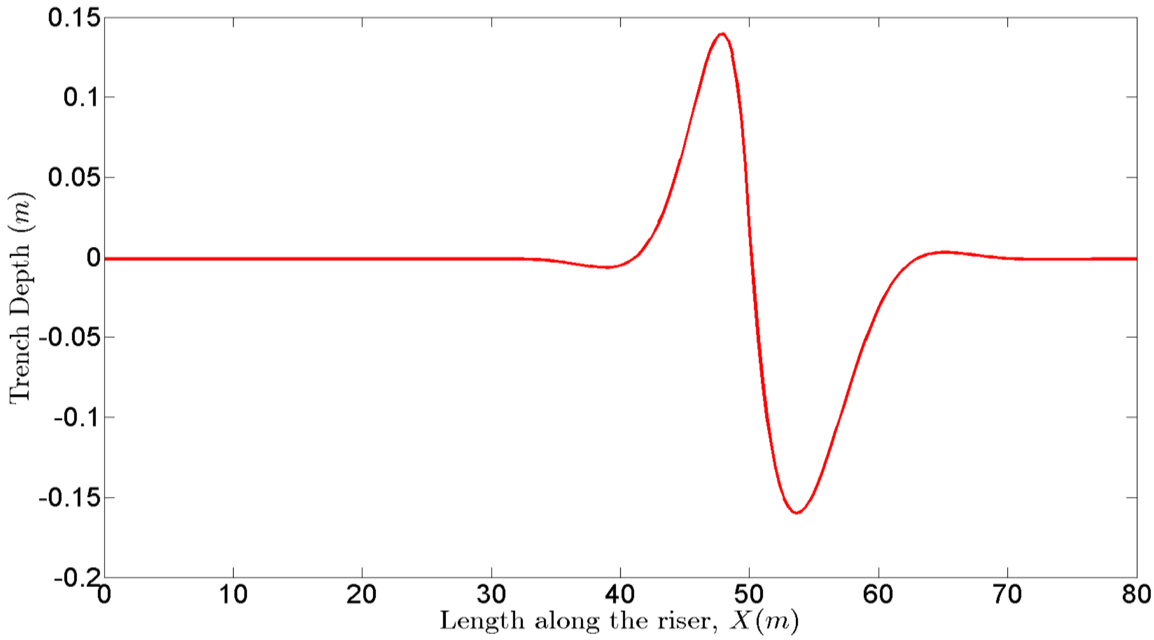

Figure 6 Riser deflected shape due to applied rotation

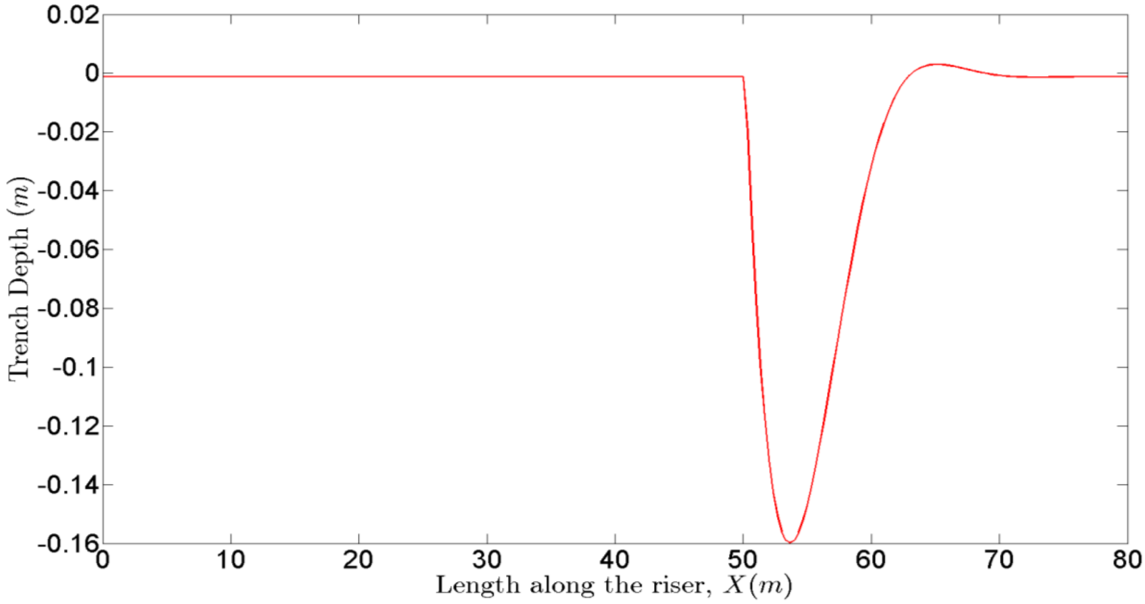

Figure 7 Trench depth reset to self-weight to the left of applied rotation

The whole process is then repeated at each node between the locations x_2 and x_1 with the rotation being released at the current node and being applied to the next (Figure 8) such that a final post-installation soil surface profile is found as illustrated in Figure 9.

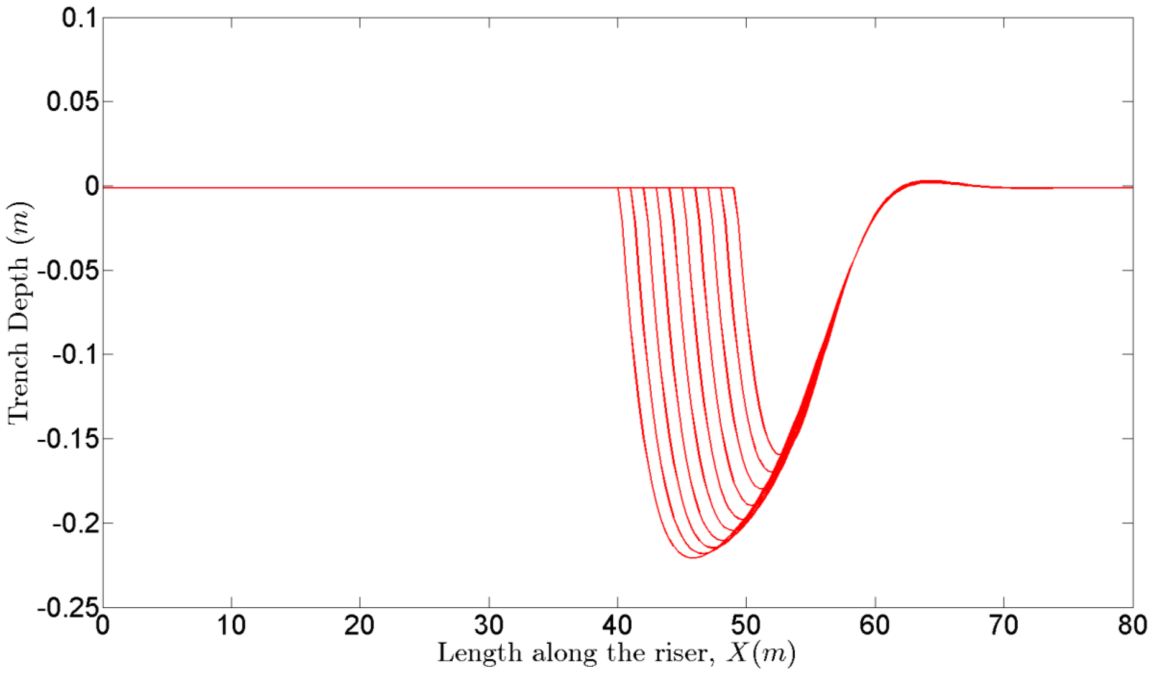

Figure 8 Trench forming as rotation is applied at each node along the riser

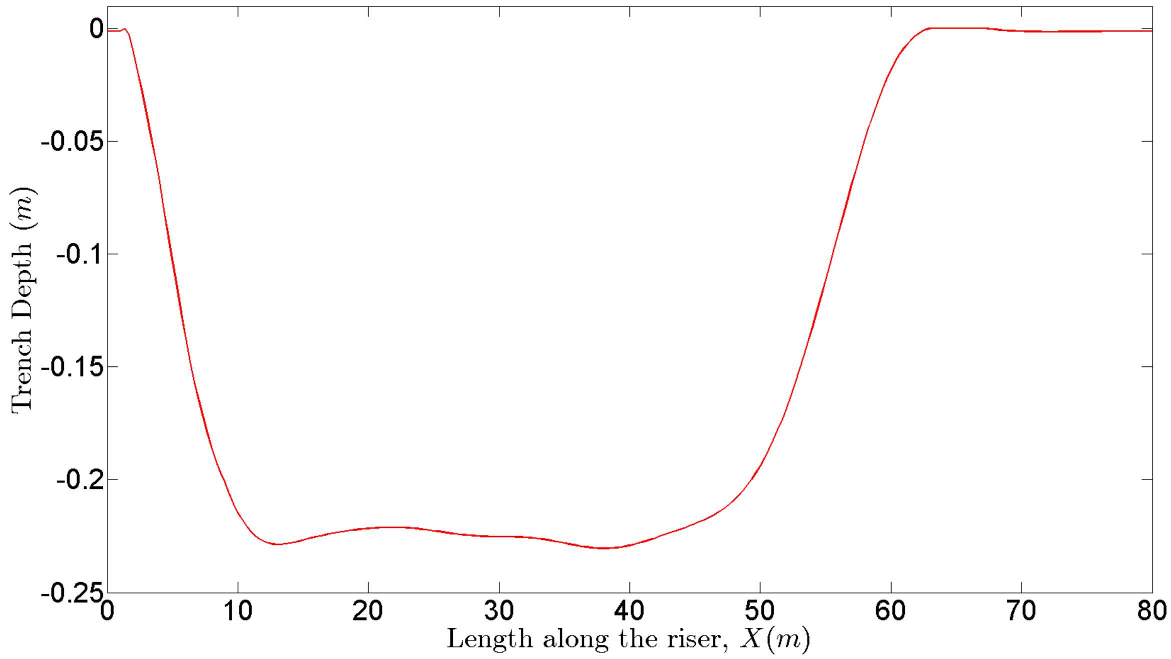

Figure 9 Final trench depth profile due to installation

3.3.1 Load-Displacement (P, y) Model

Each spring's load-displacement (P, y) characteristics follow the non-linear model illustrated in Figure 10 that was developed by Aubeny and Biscontin (2006) where P is the compressive soil resistance and y is the deflection of the riser into the soil. The model was based on the observations of laboratory model tests of vertically loaded pipes in weak sediment (Dunlap et al, 1990; Bridge et al, 2004). These tests indicated that significant soil suction occurs during uplift before the riser begins to break away from the seafloor and that this process is not a gradual one, hence the smooth curve between points B and C. Furthermore, when the displacement of the riser reverses again at point C and reconnects with the seafloor, the soil resistance is slowly mobilised as the riser penetrates the seafloor again. This is realised by the S-shaped curve between points C and E.

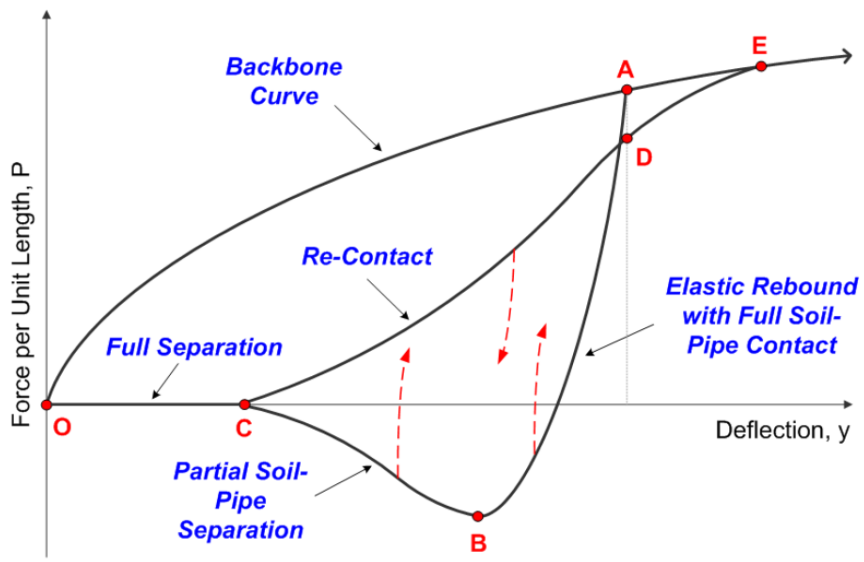

Figure 10 Degrading P-y Model (You, 2012)

Overall, the P-y model in Figure 10 includes the following components which will be discussed in more detail:

1. Virgin penetration into the seafloor characterised by the backbone curve (O-A)
2. A large deformation bounding loop (Path A-B-C-D-E) including elastic rebound with full seafloor-riser contact (A-B), uplift with partial seafloor separation (B-C) and re-contact and reloading (C-D-E) taking account of soil degradation.
3. Deflection and reversal from any arbitrary point along the bounding loop
4. Load cycles within the bounding loop

3.3.1.1 Backbone Curve

The backbone curve models the initial plastic penetration of the pipe into a virgin soil based on the collapse load computations for a horizontal cylinder of diameter D embedded in a trench of depth y. The collapse load P is related to the soil strength S_u through a dimensionless bearing factor N_p.

$$P = N_p S_u D \qquad \text{Equation 3.1}$$

In the Aubeny and Biscontin model, an empirical power law function relates the bearing factor N_p to trench depth y. This function (Equation 3.2) was developed by Aubeny, et al., (2005) where a and b are constants chosen to fit various conditions of penetration and pipe roughness. It is valid for trench depths up to $y = 5D$ and takes into consideration a non-uniform undrained shear strength profile of the form $S_u = S_{uo} + S_g z$ where S_{uo} is the undrained shear strength at the surface of the seabed and S_g is the shear strength gradient with depth whose values typically range from 0-4 *kPa* and 0-20 *kPa* respectively for soft, silty clays.

$$N_p = a\left(\frac{y}{D}\right)^b \qquad \text{Equation 3.2}$$

Equation 3.2 only consider cases where the trench width, w, equals the trench diameter D. In the case where $w/D > 1$ the maximum bearing resistance that can develop against the pipe decreases. To take this into consideration, additional relationships have been formulated which cap N_p. They will not be discussed further here, however, more details can be found in the Aubeny and Biscontin's 2009 paper.

3.3.1.2 Bounding Loop

The bounding unload-reload loop in Figure 11 occurs when the riser undergoes large cyclic loading and is characterised by elastic rebound, with full seafloor-riser contact, followed by uplift, with partial separation, and finally re-contact reloading.

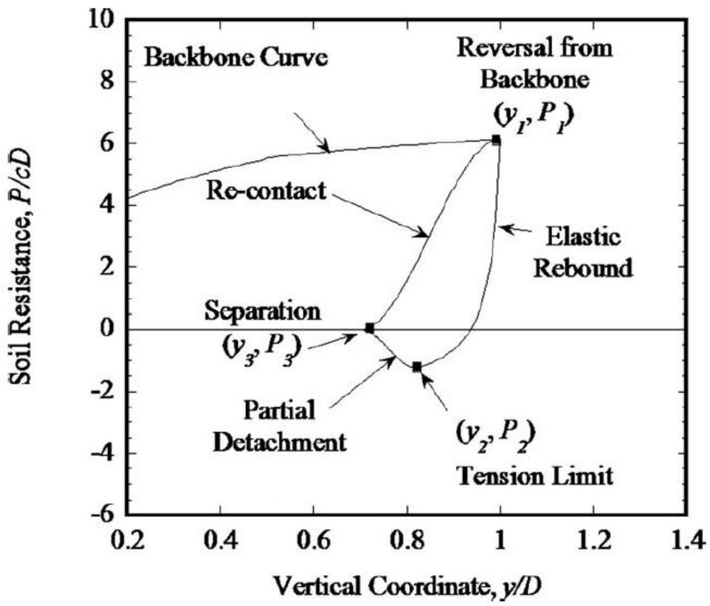

Figure 11 Non degrading P-y bounding loop (Aubeny & Biscontin, 2009)

The geometry of the loop is described by three points; (y_1, P_1), (y_2, P_2) and (y_3, P_3). Point 1, on the backbone curve, is where loading reversal first takes place. A hyperbolic relationship connects this point with point 2, the point where the maximum level of tension (suction) is mobilised during uplift. P_2 and y_2 are calculated using Equation 3.3 and Equation 3.4 respectively. Both require a model parameter ϕ that relates the maximum tensile resistance, P_2 to the maximum compressive resistance P_1. The two other model parameters k_0 and ω are estimated from laboratory model tests.

$$P_2 = -\phi P_1 \qquad \text{Equation 3.3}$$

$$y_2 = y_1 - \frac{(1-\omega)P_1}{k_0}\frac{1+\phi}{\omega-\phi} \qquad \text{Equation 3.4}$$

Point 3 is the point at which full separation between the riser and seafloor occurs. It is related to point 2 via a cubic curve described by Equation 3.5 and is calculated using Equation 3.6. Equation 3.6 requires the model parameter ψ that relates the deflection interval over which detachment of the riser occurs, to the deflection interval between points 1 and 2.

$$P = \frac{P_2}{2} + \frac{P_2}{4}\left[3\left(\frac{y-y_0}{y_m}\right) - \left(\frac{y-y_0}{y_m}\right)^3\right] \qquad \text{Equation 3.5}$$

Where $y_0 = (y_2 + y_3)/2$ and $y_m = (y_2 - y_3)/2$

$$(y_2 - y_3) = \psi(y_1 - y_2) \qquad \text{Equation 3.6}$$

Finally the S-shaped curve that reconnects point 3 with point 1 is described by Equation 3.7.

$$P = \frac{P_1}{2} + \frac{P_1}{4}\left[3\left(\frac{y-y_0}{y_m}\right) - \left(\frac{y-y_0}{y_m}\right)^3\right] \qquad \text{Equation 3.7}$$

Where $y_0 = (y_1 + y_3)/2$ and $y_m = (y_1 - y_3)/2$

Up to this point the analysis has assumed that the unloading-reloading reversal has taken place only once full separation of the riser and seafloor have occurred. In reality this could happen at any point around the bounding loop and if this is the case then deflection reversals from the bounding loop are modelled using Equation 3.8 where $\chi = 1$ for reloading, $\chi = -1$ for unloading and (y_r, P_r) refers to an arbitrary reversal point on the bounding loop.

$$P = P_r + \frac{y - y_r}{\frac{1}{k_0} + \chi\frac{(y - y_r)}{(1+\omega)P_1}} \qquad \text{Equation 3.8}$$

3.3.1.3 Cyclic Degradation

Figure 11 in §3.3.1.2 depicted a non-degrading version of the bounding loop from the original Aubeny and Biscontin model. It has since been revised to incorporate seafloor stiffness degradation effects to better simulate the seafloor's behaviour under complex cyclic loading conditions as shown in Figure 12.

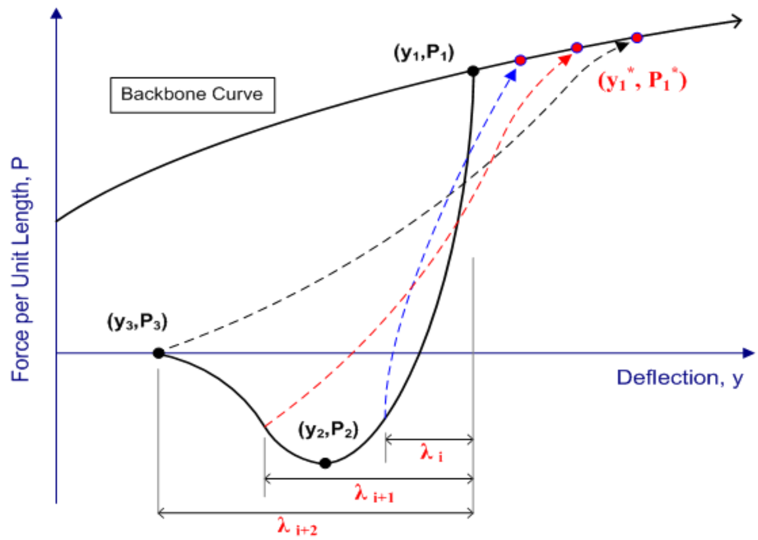

Figure 12 Degrading P-y bounding loop (Aubeny & Biscontin, 2006)

In the degrading model it is assumed that the accumulated deflection λ_n serves as a measure of energy dissipation such that

$$\lambda_n = \sum_{1}^{n} |\Delta y| \qquad \text{Equation 3.9}$$

where Δy is the incremental deflection and n is the current increment. For each incremental loading step, the apparent maximum penetration, y_1^* (also point E in Figure 10 §3.3.1) is defined as follows

$$y_1^* = y_1 + \alpha(\lambda_n)^\beta \qquad \text{Equation 3.10}$$

where y_1 is the riser pipe's deflection at the furthest reversal point on the backbone curve and α and β are degradation parameters. The parameter α mostly controls degradation in the first few cycles and β dominates as the number of cycles increases.

As the soil stiffness degrades, reloading to the same value of P results in deeper penetration so the apparent maximum load P_1^* also increases. This is expressed by the reloading curve reconnecting with the backbone curve further along than where it left off. Since P_1^* lies on the backbone curve it can be defined as

$$P_1^* = a\left(\frac{y_1^*}{D}\right)^b (S_{uo} + S_g y_1^*)D \qquad \text{Equation 3.11}$$

where a and b are the parameters defining the backbone curve (§3.3.1.1), S_{uo} and S_g relate to the soil's shear strength and D is the diameter of the riser. It is now P_1^* and y_1^* that control the bounding loop (as opposed to P_1 and y_1) and are used to calculate the other controlling bounding loop points 2 and 3 as explained in §3.3.1.2.

3.3.2 Beam-Spring Model

As shown in the flow chart in Figure 4 §3.3, after guessing an initial deflected shape of the riser due to the applied rotation, the soil resistance at each node and hence the secant stiffness k_s can be calculated using the (P, y) model just described so that a better estimate can be determined by solving the fourth-order governing differential equation for the displacement along the pipe, Δy, Equation 3.12.

$$\frac{EId^4(\Delta y)}{dx^4} + \frac{Td^2(\Delta y)}{dx^2} + k_s(\Delta y) = 0 \qquad \text{Equation 3.12}$$

This equation depends on the bending stiffness of the pipe, EI, the tension in the pipe, T and k_s which is the secant soil modulus and is a function of loading (Hetenyi, 1946).

$$k_s = \frac{\Delta P}{\Delta y} = \frac{P_j - P_{j-1}}{y_j - y_{j-1}} \qquad \text{Equation 3.13}$$

The terms P_{j-1} and y_{j-1} are the reference soil resistance and riser deflections at the beginning of the calculation step and the terms P_j and y_j are the soil resistance and deflection values computed in the current calculation step. In order to solve Equation 3.13 using a first-order central difference scheme (Hornbeck 1975) the riser is split into $(n-1)$ intervals each of length h so that it can be expressed as follows where i is an arbitrary node along the riser.

$$\begin{aligned}(y_{i-2} - 4y_{i-1} + 6y_i - 4y_{i+1} + y_{i+2}) + \frac{Th^2}{EI}(y_{i-1} - 2y_i + y_{i+1}) \\ + \frac{k_s h^4}{EI}(y_i - y_{si}) = \frac{(w_i - P_{si})h^4}{EI}\end{aligned} \qquad \text{Equation 3.14}$$

The expression can then be further simplified by rearranging the terms as shown in Equation 3.15.

$$y_{i-2} + (\alpha - 4)y_{i-1} + (6 - 2\alpha + \beta_i)y_i + (\alpha - 4)y_{i+1} + y_{i+2} = \gamma_i \qquad \text{Equation 3.15}$$

where $\alpha = \frac{Th^2}{EI}, \beta_i = \frac{k_{si}h^4}{EI} \ , \gamma = \frac{(w_i - P_{si} + k_{si}y_{si})h^4}{EI}$

For $i = 1,2, \dots n$ Equation 3.15 creates a family of equations that can be solved by linear algebra with the additional requirement of four boundary conditions that depend on the riser loading conditions. For simulating installation, the boundary conditions need to agree with applying a concentrated moment at node i along the riser. The boundary condition at point i is

$$\Delta y'(i) = \theta \rightarrow y_{i-1} = y_{i+1} - 2h\theta \qquad \text{Equation 3.16}$$

The additional three boundary conditions are related to the far field conditions. There must no displacement at both ends of the riser and a zero gradient at one end. This is achieve in practice by ensuring that the length of the riser considered is sufficiently long.

$$\Delta y(0) = y_{sw} \rightarrow y_1 = y_{sw} \qquad \text{Equation 3.17}$$

$$\Delta y(L) = y_{sw} \rightarrow y_n = y_{sw} \qquad \text{Equation 3.18}$$

$$\Delta y'(L) = 0 \rightarrow y_{n+1} = y_{n-1} \qquad \text{Equation 3.19}$$

3.4 Harbour Test

In order for the model to provide reliable results an appropriate value of the installation angle θ is required. Bridge and Willis (Bridge, et al., 2003) carried out a large scale simulation of seabed-riser interaction at the touchdown point of deep-water SCRs in Watchet Harbour in England where the seabed soil is known to have similar properties to a deep-water Gulf of Mexico seabed. Using the site geotechnical parameters summarised in Table 1 along with Bridge and Willis' observations, an estimate of an appropriate input installation angle θ could be determined using the MATLAB installation model. The harbour test consisted of a 110 *m* long, 0.1683 *m* diameter welded steel riser suspended from an actuator in the harbour wall as shown in Figure 13.

Geotechnical Parameter	Value
Moisture Content, w	$104.7\ \%$
Bulk Density, ρ	$1.46\ Mg/m^3$
Dry Density, ρ_d	$0.73\ Mg/m^3$
Particle Density, ρ_s	$2.68\ Mg/m^3$
Liquid Limit, w_L	$87.6\ \%$
Plastic Limit, w_P	$38.8\ \%$
Plasticity Index, I_P	$48.9\ \%$
Average Organic Content	$3.2\ \%$
Specific Gravity, G_s	2.68
Undisturbed Shear Strength at 1D	$3.5\ kPa$
Remoulded Shear Strength at 1D	$1.7\ kPa$

Sensitivity of Clay at 1D	3.3
Coefficient of Consolidation, c_v, at 1D	$0.5\ m^2/year$
Coefficient of Volume Compressibility, m_v, at 1D	$15\ m^2/MN$

Table 1 Harbour test seabed geotechnical parameters (Bridge & Willis, 2002)

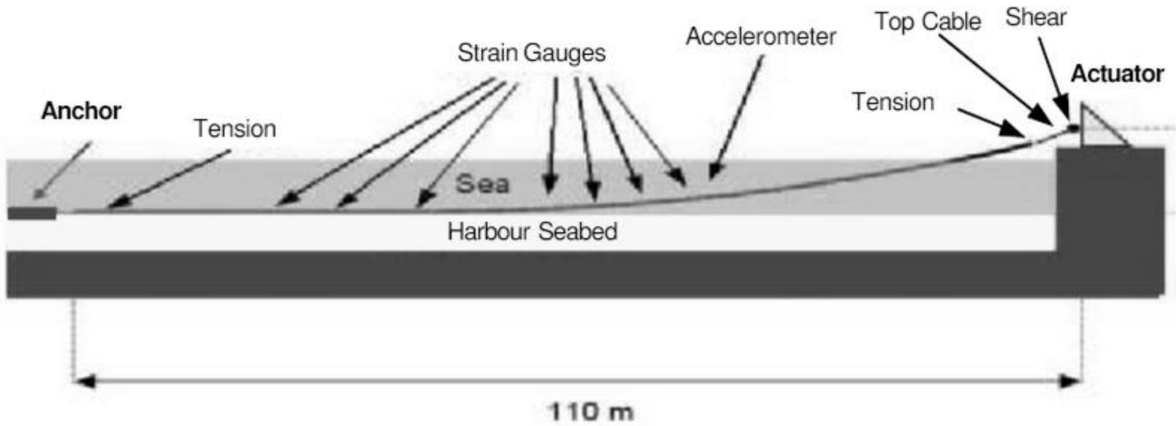

Figure 13 Harbour Test Set-Up Schematic (Bridge & Willis, 2002)

The seabed over this area was flat and undisturbed, there were no hidden obstacles below the mud line and the current velocity in the test area as the harbour filled or emptied was almost negligible meaning that any trenches formed by testing were unaffected over numerous tide cycles by scour and sediment transport. Table 2 summaries the test rig parameters.

Test Rig Parameter	Value
Pipe outer diameter	$0.1683\ m$
Wall thickness	$6.9\ mm$
Pipe material	APL 5L Grade B, $448.2 \times 10^6\ N/m^2$ yield
Height of nominal position above seabed	$9.65\ m$
Length of chain at actuator	$3.85\ m$
Length of pipe	$110\ m$
Mean water level	$3.5\ m$

Table 2 Summary of Test Rig Parameters (Bridge & Willis, 2002)

The tests were conducted over a 6 week period on numerous test corridors including an open trench. It was observed that the open trench was tear-drop in shape with a maximum depth and width that increased over the 6 week period from 0.5D - 1.2D and 1D - 2.5D respectively (Bridge, et al., 2003). Therefore it was assumed that installing the riser resulted in a trench 0.5D deep.

The appropriate soil and riser properties were input into the MATLAB model and the riser was subjected to rotations ranging from 0 radians to 1.5 radians at one end in order to determine the relationship between maximum trench depth and riser diameter. Figure 14 shows the results of this computational test. These results show that the relationship between the vertical displacement and applied installation angle is linear such that

$$\frac{Max\ trench\ depth}{Riser\ diameter} = 5.42\theta \qquad \text{Equation 3.20}$$

Thus to achieve a maximum trench depth of 0.5D the installation angle required is 0.09 radians. This is equivalent to 5.16 degrees.

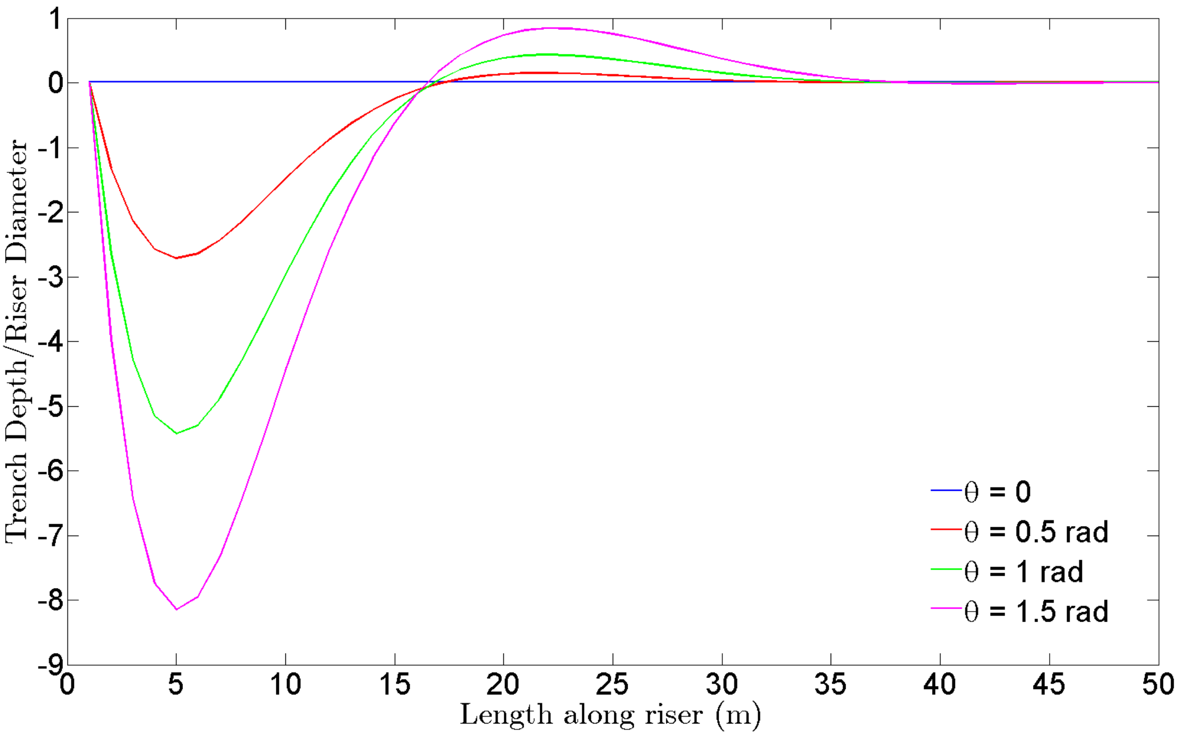

Figure 14 Riser shape when subject to rotation at one end of the riser

4 Results and Discussion

4.1 Installation angle

4.1.1 Effect of varying installation angle on trench depth

To verify that the estimate for the installation angle, θ, calculated using the harbour tests is valid the installation model was run for angles ranging from 0.07 to 0.11 radians and compared to the post-installation trench field observations carried out by Bridge and Howels (2007). The model parameters selected represent a generic soil with realistic properties. Table 3 summaries the test parameters used.

Type	Parameter	Symbol	Value
Material	Pipe diameter	D	$0.15\ m$
	Wall thickness	t	$0.0069\ m$
	Modulus	E	$1.93\ GPa$
	Mud-line shear strength	S_{uo}	$2\ kPa$
	Shear strength gradient	S_g	$5\ kPa/m$
	Initial stiffness	k_0	1200
Bounding Loop	Power law coefficient	a	6.8
	Power law exponent	b	1.2
	Maximum uplift load	ω	0.65
	Uplift load limit	ϕ	0.2
	Breakout	ψ	1.2
Degrading	Re-penetration	α	0.7
	Re-penetration	β	0.25
	Degrading rate	μ	0.01
	Degrading rate	ϵ	0.45
	Initial load drop	Ω	0.35
Interaction	Number of nodes	n	$201\ (0.5\ m)$
	Maximum iteration	-	100
	Tolerance	η	0.00001
Installation	Axial tension	T	$100\ kN$

	Installation angle	θ	$variable$
	Penetration rate	v	$0.05\ mm/sec$

Table 3 Model Test Parameters

The tests were carried out on a 100 m long steel riser to which the installation process was run from x_2 = 80 m to x_1 = 10 m. The main reason for beginning and ending the simulations away from the very ends of the riser was to prevent the boundary conditions enforced at these points affecting the results. Additionally by starting the simulation at x_2 = 80 m the visualization of the effect of the rotation beyond this point was possible.

Figure 15 shows the effect that varying the installation angle has on the trench profile. It demonstrates that the maximum trench depth increases linearly with installation angle. This relationship is as expected because as the angle is increased, the riser is forcibly pushed further into the seabed. The ranges of trench depths observed in the catenary and buried zone by Bridge and Howells (2007) on SCRs in the Gulf of Mexico and off the coast of Brazil were between 2.5D - 5D deep. As the range of depths predicted by the model is similar to the range of those observed in the field it can be concluded that 0.09 radians is a sensible value of θ to use in order to accurately model the installation process.

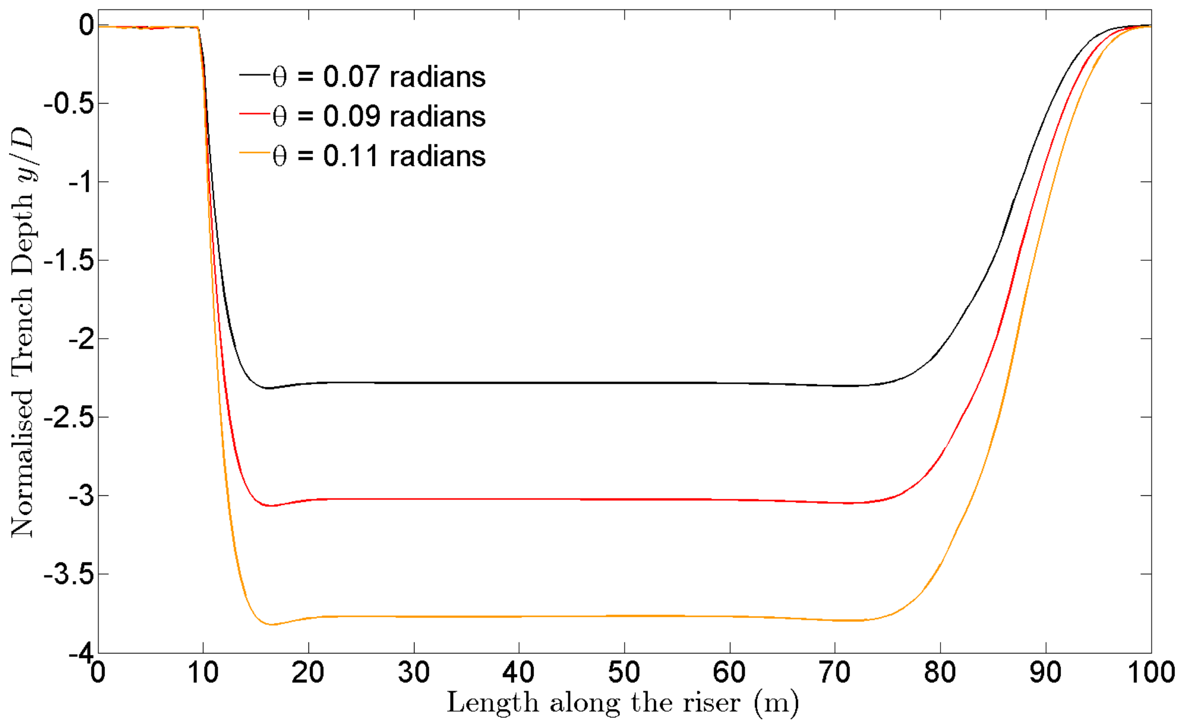

Figure 15 Normalised trench depth for a range of installation angles

4.1.2 Effect of varying installation angle on moment envelope

Figure 16 shows the moment envelope along the riser during installation for a range of installation angles. Overall the maximum hogging and sagging moments are linearly proportional to the installation angle applied. This is because a larger rotation induces greater curvatures along the SCR and hence greater bending moments. Note also that the hogging moments are smaller than the sagging ones as during installation the curvatures experienced by the riser in the hogging sense are much smaller than those in the sagging sense.

Furthermore the central part of the graph indicates a constant moment envelope between the locations on the riser where installation process was run. This suggests that the application of the rotation at each node causes the large maximum sagging and hogging moments in the riser. Therefore when choosing between the J-lay or S-lay installation methods it is important to select the one that keeps the installation angle as shallow as possible to minimise the moment envelope.

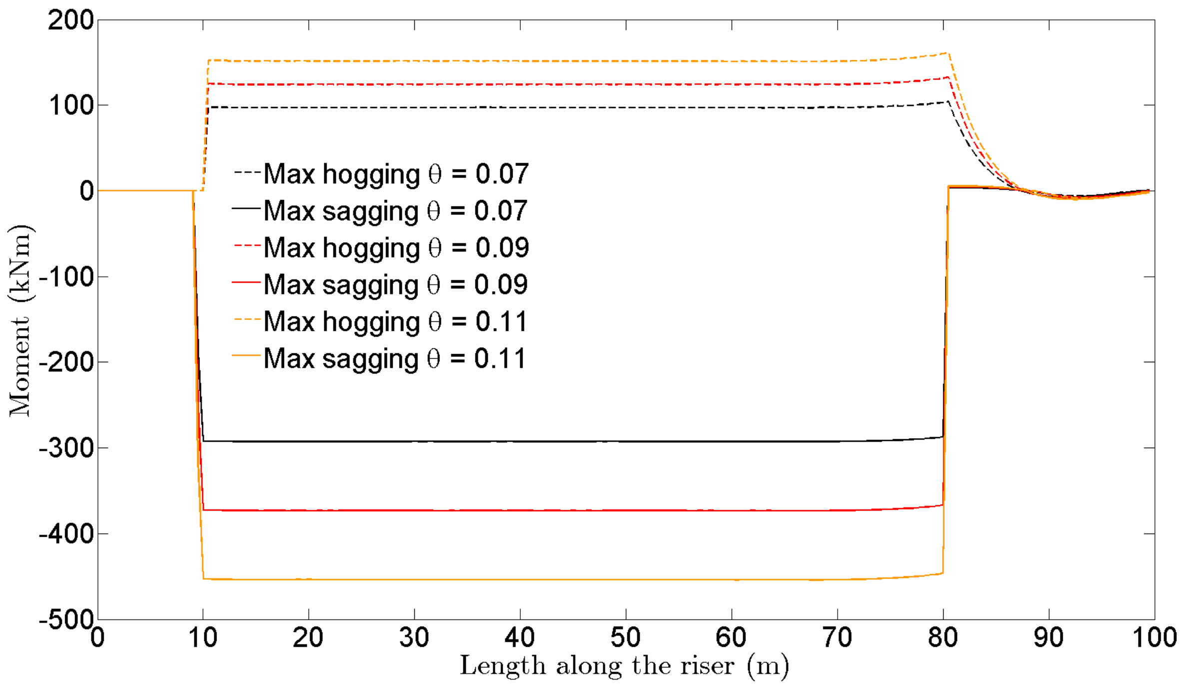

Figure 16 Moment envelope for a range of installation angles

4.1.3 Combining installation and displacement loading

It is also of interest to see what effect installation has on bending moments and trench formation when the riser is subject to operational loading. This was analysed by running the installation process from x = 50 *m* to x = 0 *m* along a 100 *m* riser and then applying twenty cycles of the saw-tooth loading shown in Figure 17 at x = 0 *m*. Figure 18 shows the lay-up lay-down profile of the riser during one cycle of this loading.

The reason why, in this set-up, the installation process is being run to the very end of the riser despite previous concerns about the boundary condition affecting the bending moment profile, is because currently the model can only apply vertical displacement loading at one end of the riser and not part way along it. Therefore if the installation process was halted at some point before the end of the SCR, the displacement loading would not be applied to a section of the riser laying in the trench formed by installation and the effect of it would not be apparent. Fortunately, for this analysis, only the moment range during the application of the working load is of interest so the bending moments computed for the riser as it undergoes installation can be neglected.

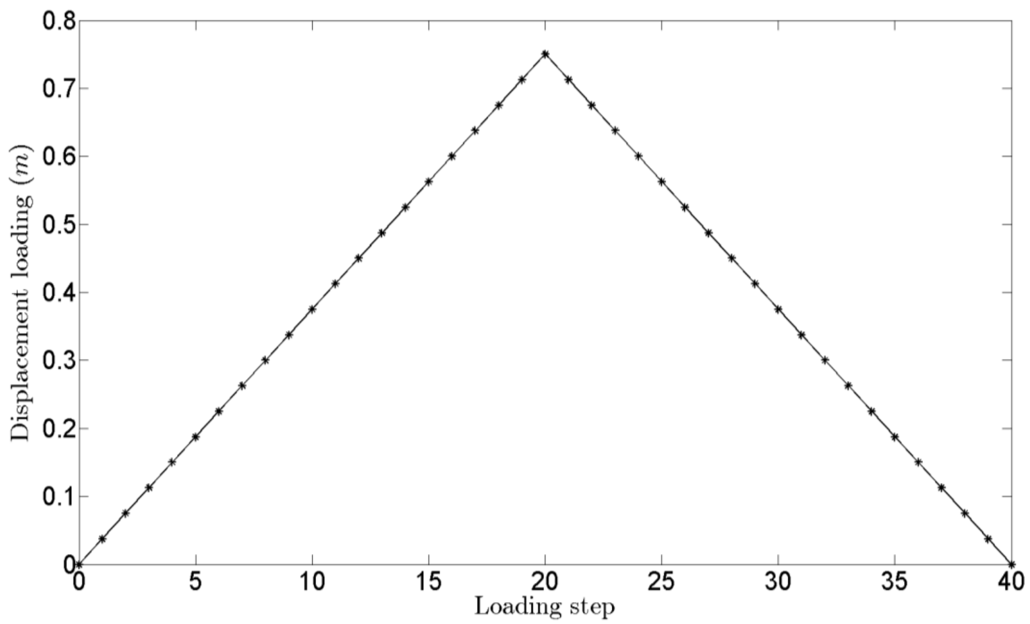

Figure 17 A single cycle of saw-tooth loading history applied at x = 0 m

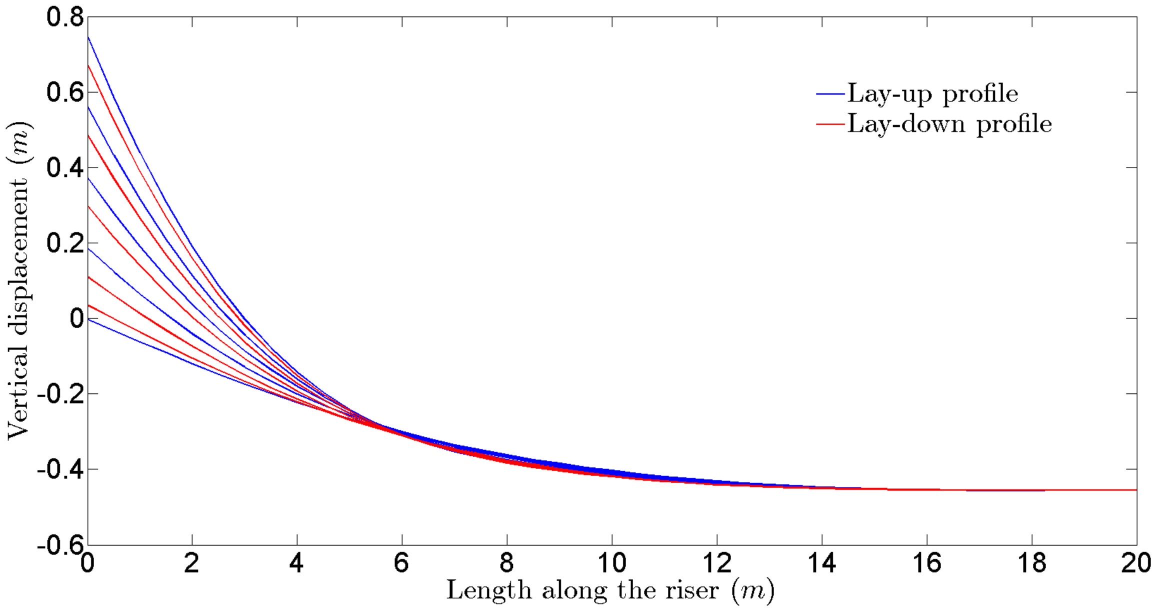

Figure 18 Lay-up and lay-down profile of riser for displacement loading history

Figure 19 shows the final trench profiles for different combinations of installation and operational loading. What can be seen from the figure is the large impact that including installation has on final trench profile after the riser has undergone 20 cycles of the saw-tooth loading. The maximum trench depth is approximately 6 times greater when installation is

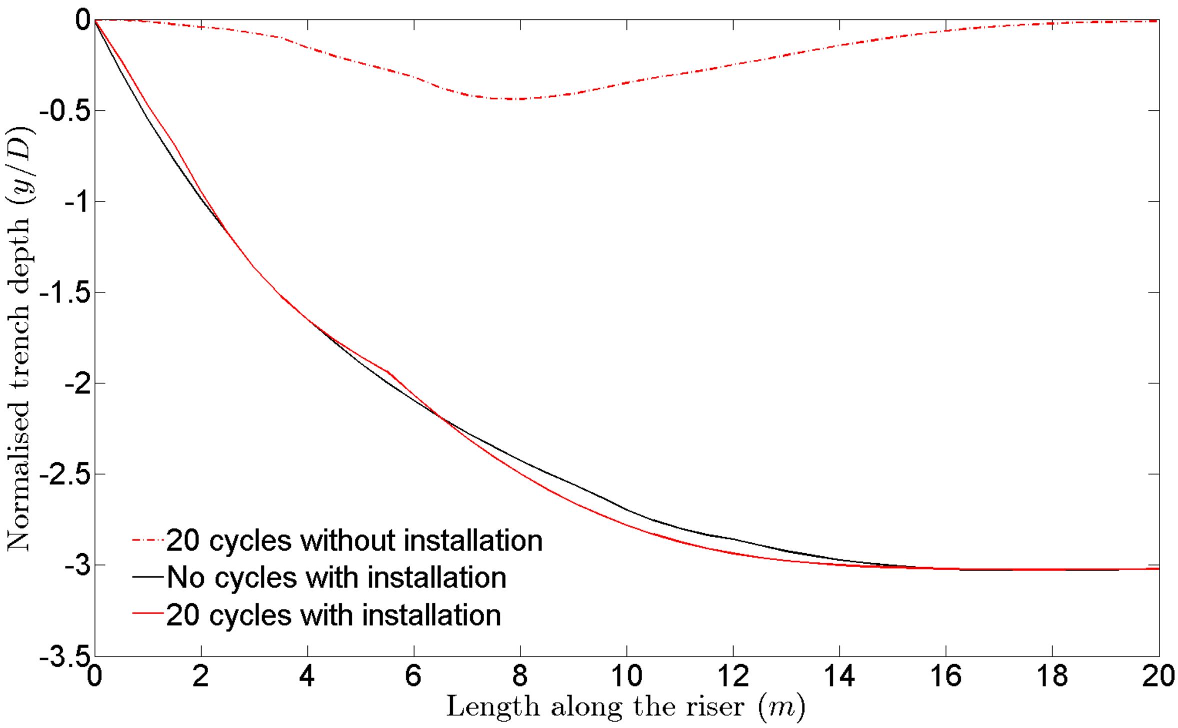

Figure 19 Normalised trench depth for various combinations of installation and operational loading

taken into consideration and the change in trench depth profile as a result of the loading is much smaller. This is as expected because during the installation process a deep initial trench is created and the soil resistance at this depth is greater than that at the surface of the seabed.

Figure 20 shows the bending moment profile along the riser for the same twenty cycles of saw-tooth loading with and without installation. Both the maximum and minimum moments experienced by the riser increase when installation is taken into consideration. The maximum moment increases by 4.5% from 88 *kNm* to 92 *kNm*. This has a detrimental impact on the riser's fatigue life and indicates that current predictions, that neglect installation loading, may not be conservative. Additionally, this main increase occurs at a location where the maximum trench depth has not yet been reached, therefore, one would expect that if the same loading were to be applied to a riser laying at maximum depth then the percentage increase in bending moment would actually be larger than this and the reduction in fatigue life even greater.

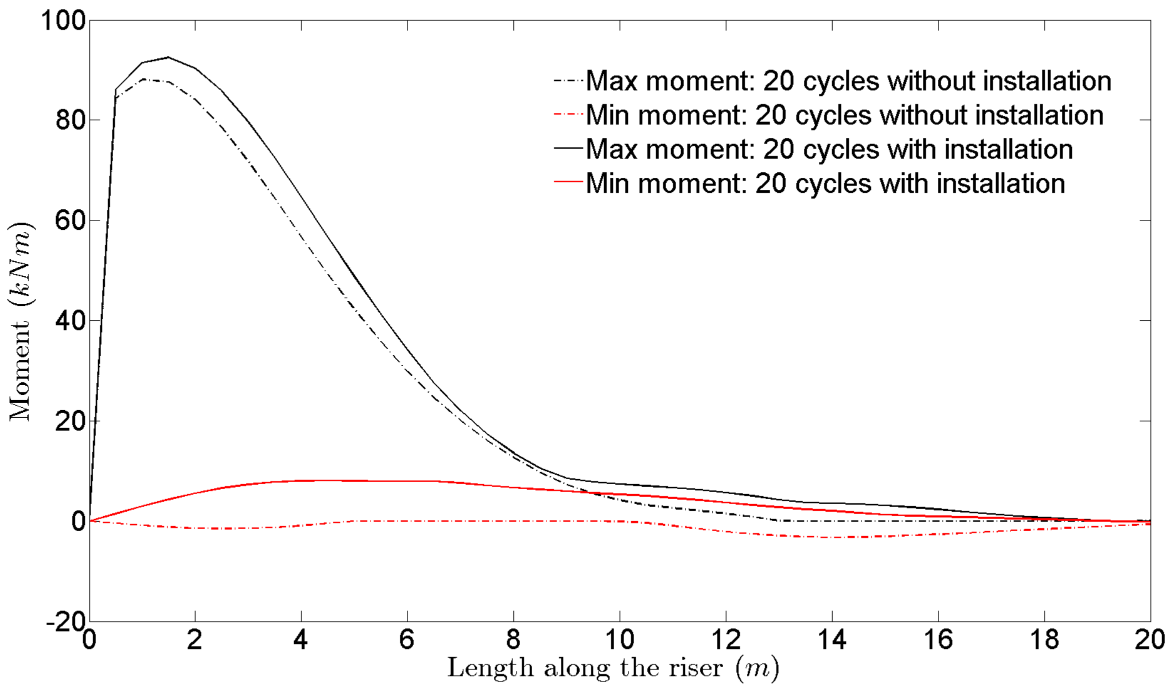

Figure 20 Bending moment envelope for 20 cycles of operational loading with and without installation

One final thing worth investigating is the impact that the installation angle used has on the difference between working load bending moments post-installation. Figure 21 shows the maximum bending moment profile along the riser for a range of angles. It illustrates that the

effect of changing the installation angle, although less critical than deciding to include installation, is still significant and increasing θ increases the maximum bending moment.
As it may be challenging to determine an accurate, site specific, value of θ it is advantageous to know that an estimate should suffice and not drastically affect the reliability of the model output.

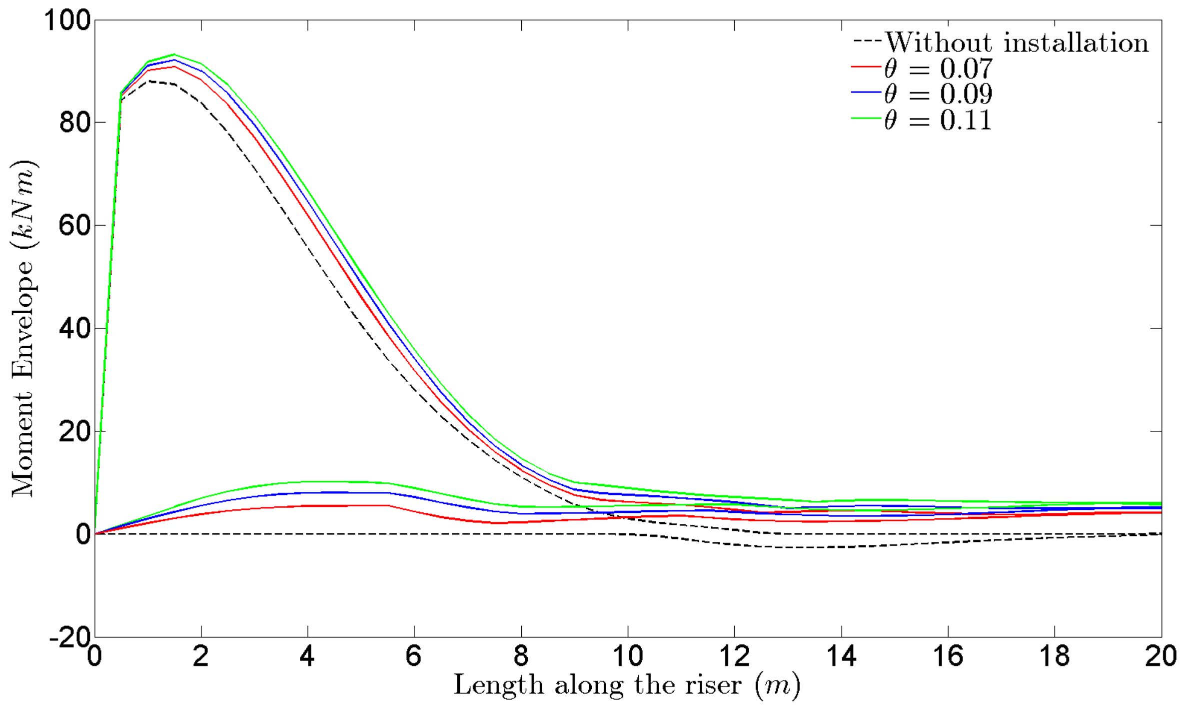

Figure 21 Working load bending moment envelope for range of installation angles

Overall these results demonstrate the importance of including the effects of installation when predicting the operational bending moments and hence fatigue life of an SCR more accurately. Furthermore it can be seen by comparing the bending moments in Figure 21 with the bending moment envelope during installation (Figure 16) that these operational moments are approximately an order of magnitude smaller than the moments the riser experiences during installation. This confirms that installation is one of the most critical loading scenarios for an SCR.

4.2 Parametric Study

Having shown that including the installation loading increases the riser's working life bending moments it is worthwhile looking into the effect that other model parameters have. The two parameters that will be looked at in more detail are the riser's diameter and penetration rate.

The same basic model parameters for a generic soil will be used in this analysis as outlined in Table 3 §4.1.1.

4.2.1 Effect of varying riser diameter

4.2.1.1 Trench Depth

Figure 22 shows the normalised trench profile after installation for a range of riser diameters. The trend is that the maximum trench depth increases with riser diameter. This is because during installation the load-deflection relationship mainly follows the backbone curve model outlined in §3.3.1.1 where the soil resistance $P \propto D^{-0.2}$. Hence as the riser's diameter increases, the soil resistance decreases and deeper trenches are created. This trend is supported by two independent field observations, outlined in Table 4, of post-installation trench depths both in clays with very similar properties to Gulf of Mexico clay.

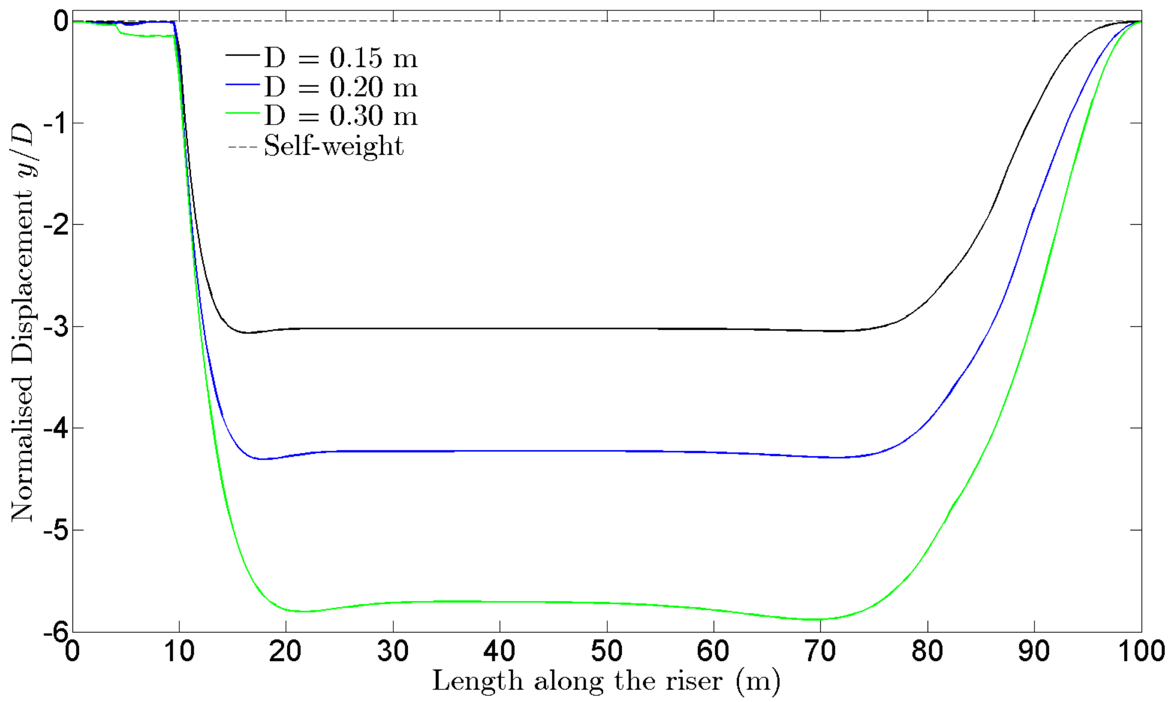

Figure 22 Normalised trench profile after installation varying diameter

Test	Riser Diameter, D (m)	Maximum trench depth
Harbour Test (Bridge & Howels, 2007)	0.17	0.5D
Gulf of Mexico (Bhat, et al., 2013)	0.30	3D

Table 4 Post-installation trench depth field observations

The observations summarised in Table 4 can also be compared to the 0.15 m and 0.30 m riser model results. Overall the model predicted deeper trenches than those observed. For example the observed trench depth for the 0.15 m riser was 0.5D however the model predicted a trench 3D deep. The reason for this large discrepancy is that the harbour test clay and the Gulf of Mexico clay have a higher value of undrained shear strength at the seabed S_{uo} than that used in the model (approximately 4 kPa in comparison with 2 kPa). Thus the model provided less resistance against trench formation and deeper trenches were predicted.

Finally, Figure 22 also shows that as the riser diameter increases, the length of the riser from the last applied point of rotation (x = 0 m) to the location at which the maximum trench depth is reached increases. For example, when D = 0.15 m the maximum trench depth is reached at approximately x = 15 m but when D = 0.30 m this occurs at x = 20 m. This can be explained because the riser's bending stiffness increases with diameter and so larger risers will resist the applied installation more resulting in the maximum trench depth occurring further from the applied rotation. Figure 23 supports this explanation by illustrating the effect that varying the bending stiffness of the riser, while applying a rotation of 0.09 radians at x = 0 m has on the maximum trench depth and its location.

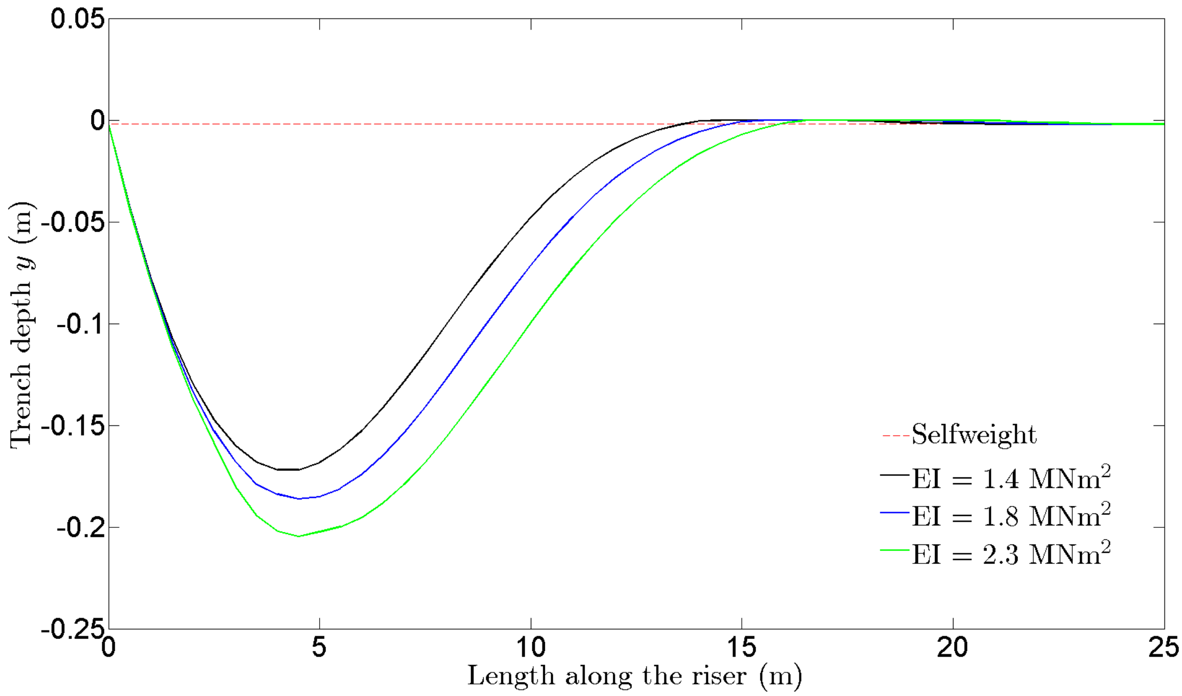

Figure 23 Trench profile for a range of bending stiffness'

4.2.1.2 Moment Range

Figure 24 shows the moment envelope experienced during installation by risers with diameters ranging from 0.15 *m* to 0.3 *m*. As the diameter increases, so does the minimum and maximum bending moments. The reason for this non-linear relationship is that as the installation angle is increased and deeper trenches are formed, as a result of the linearly increasing shear strength profile, the soil resistance increases resulting in larger bending moments. It is therefore recommended that the riser diameter is kept to a minimum in order to reduce the bending moments experienced by the riser during installation, prevent yielding of the material and prevent the formation of residual stresses.

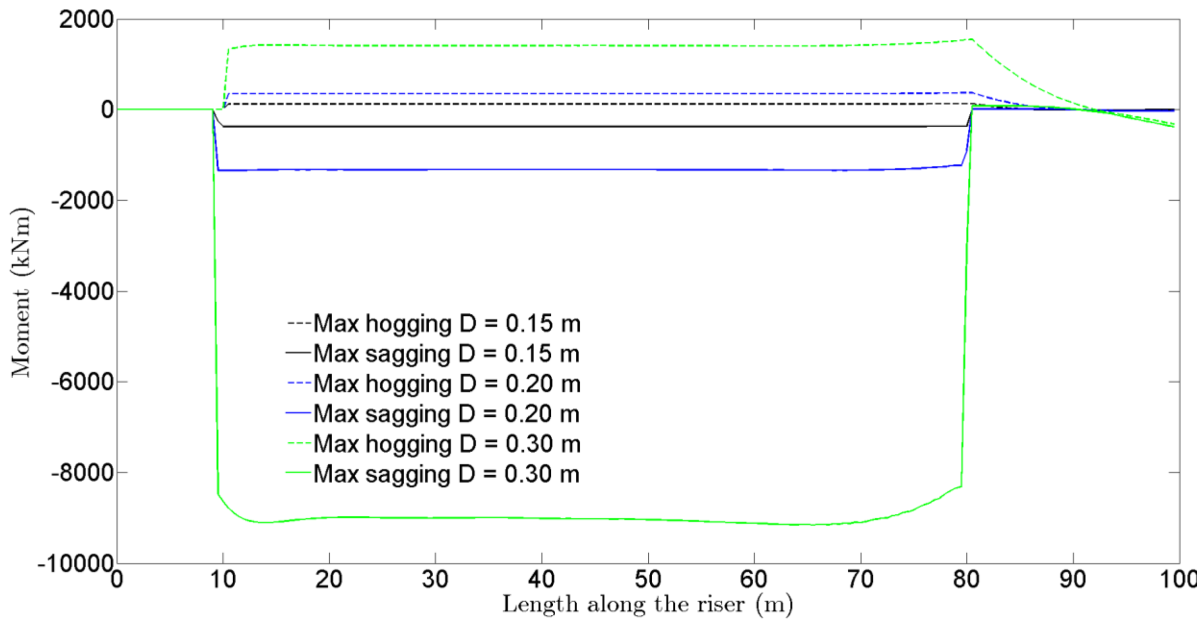

Figure 24 Moment envelope for a range of riser diameter's

4.2.2 Effect of varying penetration rate

4.2.2.1 Model Calibration

Apart from installation another thing lacking in the seafloor-riser interaction model developed by Aubeny and Biscontin is that it cannot directly take account of the penetration rate of the riser into the soil because the equations it is based on are independent of time. In order to try and take account of this indirectly, soil model parameters were calibrated so that the model output for a specific loading history matched, to as great an extent as possible, two large-scale physical model tests carried out the by the Norwegian Geotechnical Institute (NGI) in collaboration with Langford & Aubeny, (2008).

These two single stage cyclic tests aimed to investigate the effect of penetration rate on seafloor-riser interaction in the touchdown zone. They were carried out on model pipes of length 1300 mm and diameter 174 mm, on re-constituted high plastic marine clay with a soil profile of 2 kPa at the seabed and strength gradient of 13 kPa/m. The first test was run at a penetration rate of 0.05 mm/s and the second test at the faster rate of 0.5 mm/s. During each cycle the pipe was penetrated to a constant level of soil resistance: about 9.5 kPa for Test 1 and 11 kPa in Test 2, before being lifted to the point of full soil-pipe separation in order to obtain a complete picture of the suction plateau. There were three model parameters that were of interest when calibrating the model with these tests: ω, ϕ and ψ.

1. The effect of ω on the model response is shown in Figure 25. It is used to determine the change in displacement required to pass from the maximum compressive resistance to maximum tensile resistance on the bound loop. A larger value of ω results in a smaller change in displacement to pass between these limits and hence a wider bounding loop.

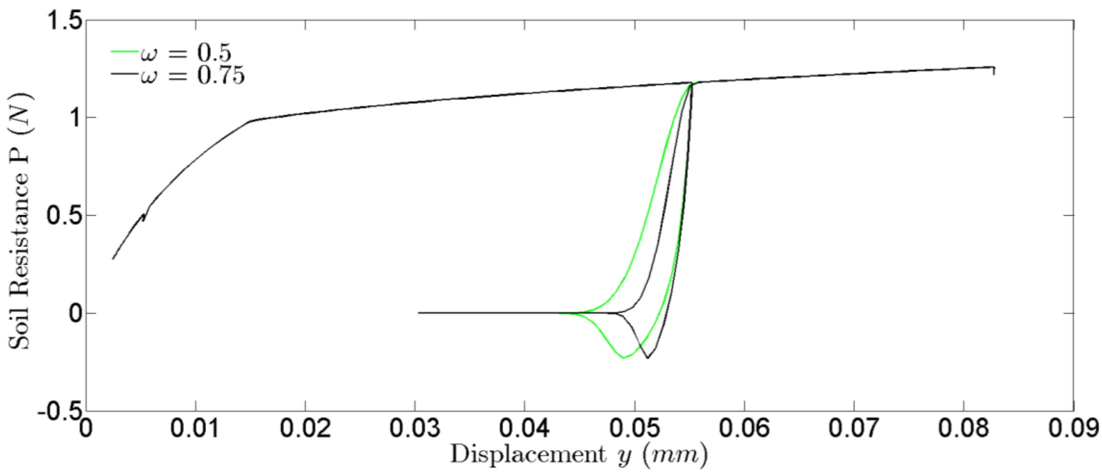

Figure 25 Effect of ω on bound loop

2. In a similar vein, ϕ is used to relate the maximum compressive resistance on the bound loop to the maximum tensile resistance as seen in Equation 3.6, §3.3.1.2. A larger value of ϕ results in a higher tension limit and larger bounding loop as can be seen in Figure 27.

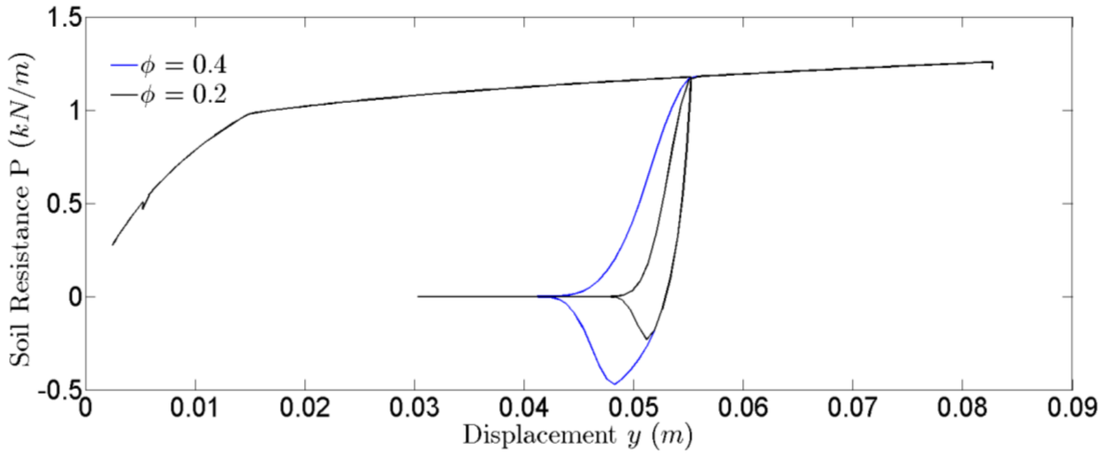

Figure 27 Effect of ϕ on bound loop

3. Figure 26 shows the effect of the parameter ψ on the model response. ψ is used to determine the point where the pipe becomes completely detached from the seabed and therefore controls how the uplift force decays as seen in Equation 3.6, §3.3.1.2. A larger value of ψ results in a later detachment of the riser from the seabed and therefore a wider bounding loop.

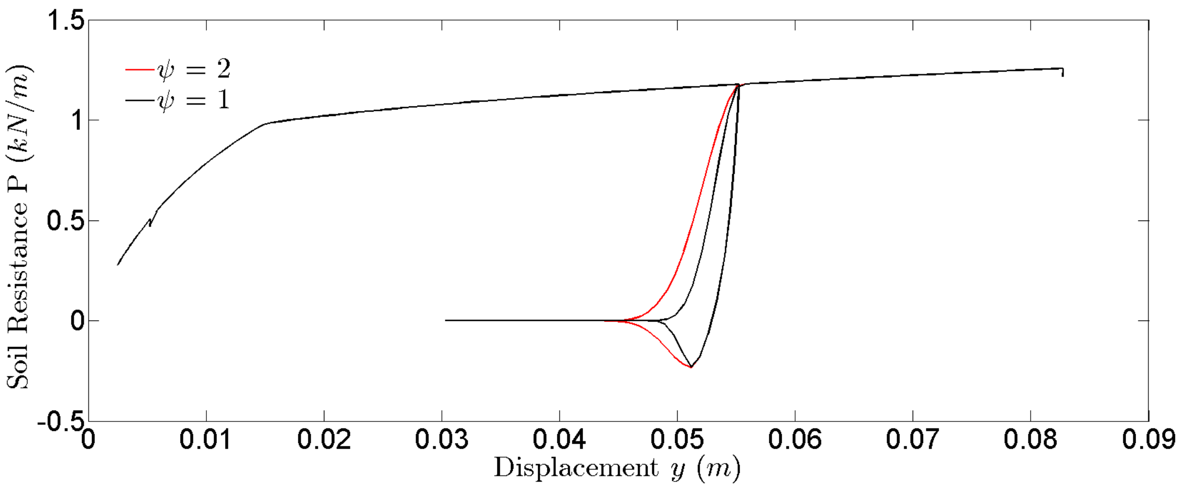

Figure 26 Effect of ψ on bound loop

Figure 28 and Figure 29 show the large-scale model testing load-displacement curves for the two NGI large scale tests compared with the model output for penetration rates of $0.05\ mm/s$ and $0.5\ mm/s$ respectively. Table 5 summaries the different values of the degrading parameters just described to calibrate the model to the large-scale test results.

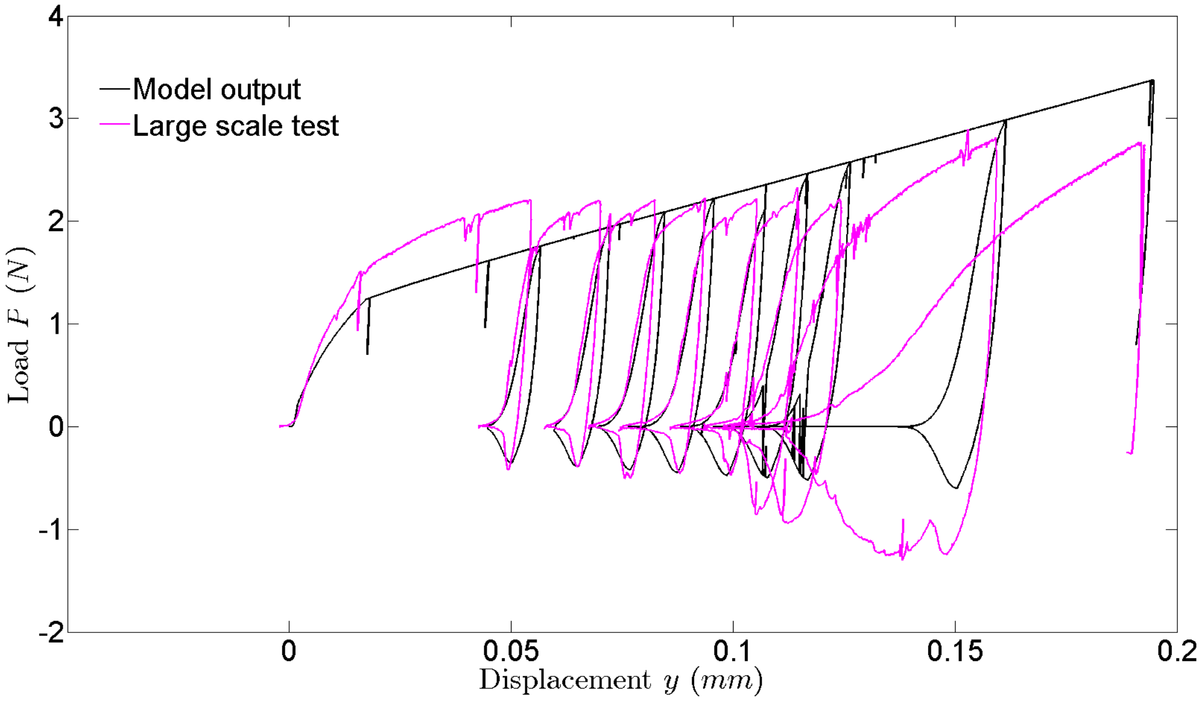

Figure 28 Test 1 penetration rate v = 0.05mm/sec

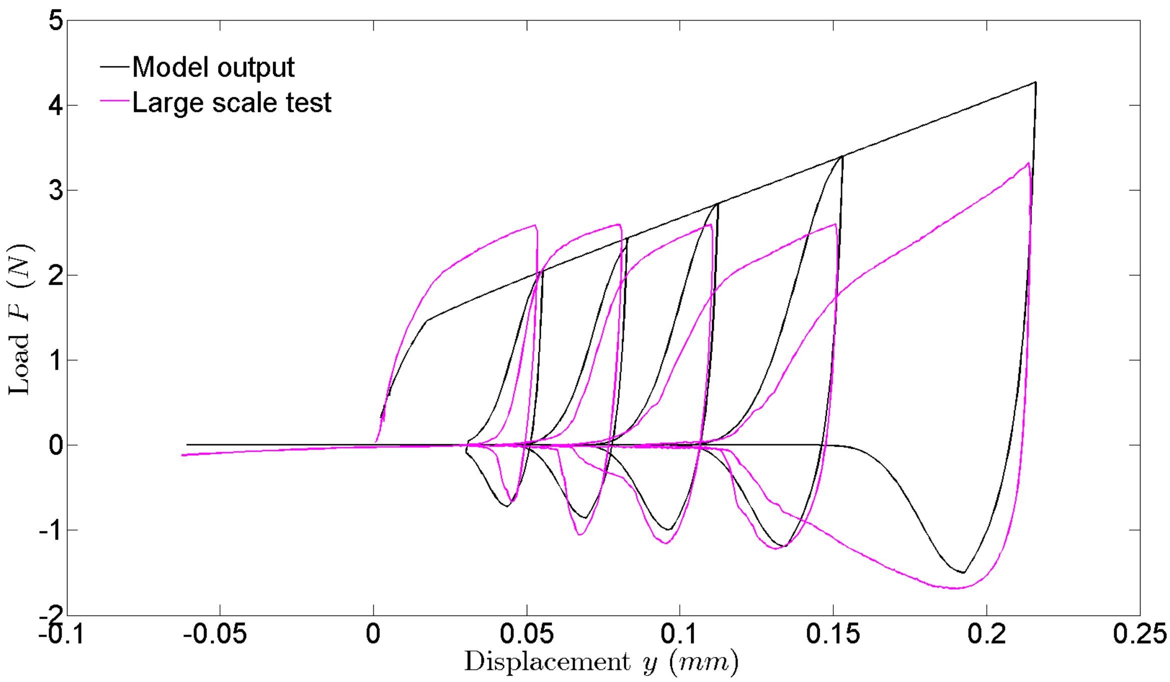

Figure 29 Test 4 penetration rate v = 0.5 mm/sec

Model Parameter	Test 1 v = 0.05mm/s	Test 4 v = 0.5mm/s
$\boldsymbol{\phi}$	0.20	0.30
$\boldsymbol{\psi}$	1.20	2.00
$\boldsymbol{\omega}$	0.65	0.70

Table 5 Summary of affect model parameters for differing penetration rates

Overall, in particular for the first few cycles, the model and large scale tests produce fairly similar results. However as the number of cycle's increases, the model fails to capture the behavior of the soil when subject to tensile loading and neither does the backbone curve model fit the large scale test data well. Despite these inadequacies, the model parameters determined to represent the two different penetration rates should be sufficient to qualitatively compare the effect of penetration rate on installation trench depth and moment envelope.

4.2.2.2 Effect of penetration rate on the shear strength of clay

There are two main mechanisms which affect the strength and hence response of a clay as a result of the penetration rate. Firstly the closer the conditions are to fully drained during penetration, the higher the value of soil resistance because if the penetration is sufficiently low that the soil ahead of the penetrating object has time to consolidate, then larger shear strength and stiffness' are developed than would have done under undrained conditions. Secondly, in soils with high clay content in fully undrained conditions, the greater the penetration rate, the larger the undrained shear strength S_{uo}. (Kim, et al., 2008).

Consequently one would expect that increasing the penetration rate would result in greater soil resistance and bending moments but shallower trenches. Similarly, the degrading parameter ω would increase because the change in displacement required to pass from maximum compressive to tensile resistance on the bound loop would reduce. One would also expect a larger tension limit and a greater displacement required for complete detachment of the riser of the soil leading to an increase in the values of ϕ and ψ. The values in Table 5 support this theory as the parameters calibrated for Test 2 that had the faster penetration rate are larger than those for Test 1.

4.2.2.3 Trench Depth

Figure 30 shows that increasing the penetration rate during installation reduces the trench depth which agrees with the theoretical prediction. Moreover it is interesting that increasing the penetration rate by a factor of ten causes only a 10% reduction in trench depth. Therefore, it can be concluded that, comparatively, the penetration rate does not have as big an impact on the final installation trench depth as both installation angle and riser diameter. Finally Figure 30 suggests that increasing the penetration rate results in a more uneven trench profile. However it is likely that this is not a function of the penetration rate but of the fineness of the mesh used for the finite difference analysis. The nodal spacing used for all tests throughout this report is 0.5 m which is quite large. The reason for not using a finer mesh is due to the time that the computation analysis would have taken. Therefore, if a finer mesh were used then one would expect the trench profile for the higher penetration rate to be more uniform.

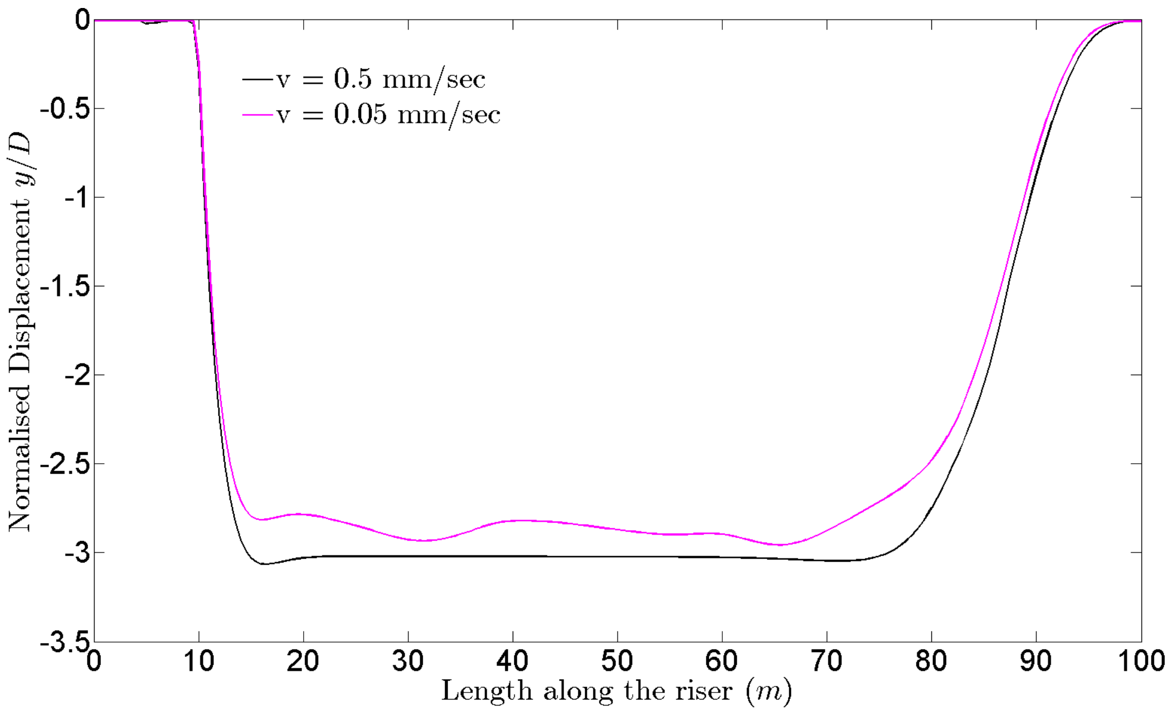

Figure 30 Normalised trench depth when varying penetration rate

4.2.2.4 Moment Range

Figure 31 shows that the moment envelopes experienced by the riser for the two different penetration rates are almost identical. This is unsurprising because the bending stiffness' of both the risers were identical as was the installation angle and therefore the curvatures experienced would have been very similar. Again, the probable reason for the unevenness of the bending moment profile is due to the large nodal spacing along the SCR.

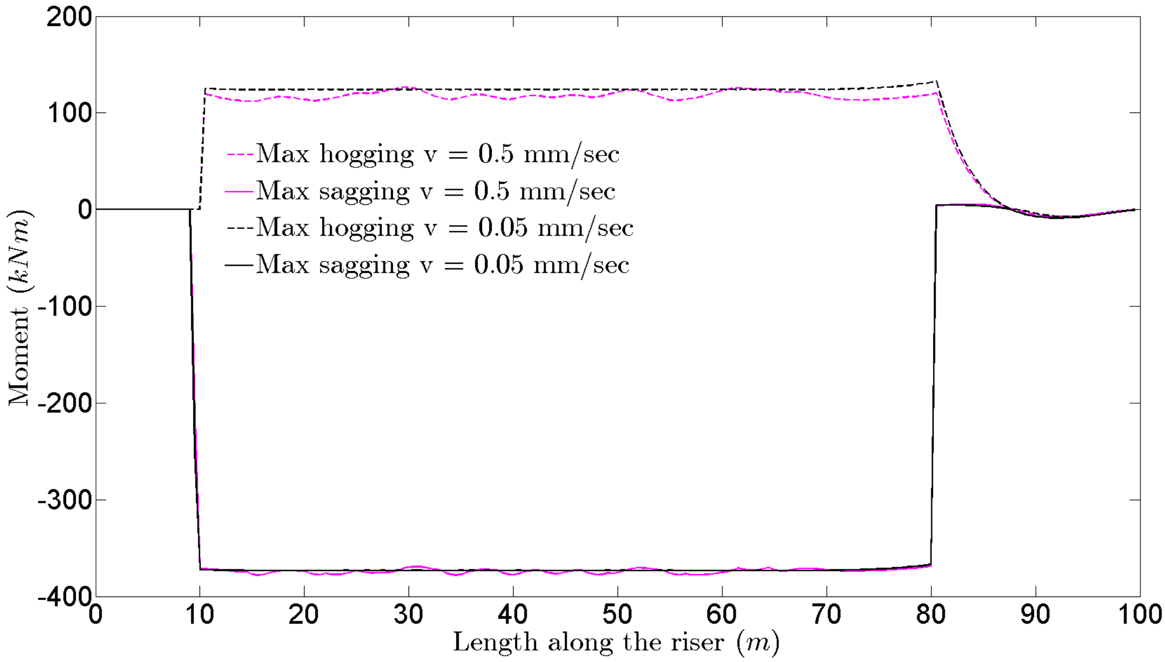

Figure 31 Moment envelope along the riser for when varying penetration rate

4.3 Design Recommendations

Using the research carried out in this report a number of design recommendations can be made. Firstly results have shown that is important to minimise the installation angle to keep the bending moments during installation and post-installation as small as possible. Additionally, risers with smaller diameters reduce the post-installation trench depth and bending moments and hence increase the fatigue life of the riser. However, when choosing the riser diameter size it is important to make sure that it is not too small so that the flow rate of the oil through the pipe will not exceed a sensible limit. Finally any time that an oil rig spends not in operation is very costly so it is advantageous that a high laying rate has a positive effect on the fatigue life of the SCR.

4.4 Critical Evaluation of the Model

Advantages

The seafloor-interaction model can account for all phases of interaction including non-linear soil behaviour, soil suction and breakaway, soil yielding, and degradation under cyclic loading. It is very versatile as any combination of imposed displacements, tension and moments can be applied and the resultant trench formation and bending moments can be predicted. This allows for both the modelling of general loading during the working life of the riser as well as facilitating the installation process. Including the installation process in the program allows for a more realistic prediction of trench depth and bending moments during the life of a SCR and highlights the critical nature of the loading it is subject to during installation. Finally the model has been designed with the view of creating a package that is easily accessible to designers and can be run on a personal computer. It allows for the manual input of a large of riser and soil properties to enable the output to be tailored to specific sites and scenarios.

Disadvantages

Determining the backbone curve and bounding loop parameters used in the model require special laboratory tests involving instrumented pipes penetrating into a clay-filled test basin. Measurements collected during initial penetration are used to determine the two backbone parameters a and b and measurement collected during an unloading cycle can be used to determine the bounding loop parameters k_0, ω, ϕ and ψ. Also, in order to achieve better results a fine mesh with a large number of nodes would be required but, due to the long length of the riser, and the time required to iteratively solve the ordinary differential equation at each node for each time step, the time to run the code is too long to be viable. This reduces the model's value as a convenient design tool.

Future Considerations

Currently the model allows for the computation of the moments along the riser however it would be beneficial if the model could use these results to compute an estimated fatigue life of the riser. Furthermore, the incorporation of time into the model to enable the analysis of the effect of consolidation would make it even more realistic.

5 Conclusion

In conclusion this report has detailed a way to model the installation of SCRs in conjunction with the non-linear, degrading, seafloor-riser interaction MATLAB model developed by Aubeny and Biscontin (2009). It requires the manual input of the installation angle θ, and the two points along the SCR between which the installation process will be run. Observations from the harbour test carried out by Bridge and Willis (2002) allowed a realistic value of θ = 0.09 radians to be estimated. One limitation of the installation model is that in order to avoid the boundary conditions imposed at each end of the riser affecting the bending moment profile, it must be run sufficiently far away from the ends of the riser. This makes interfacing installation with future loading on the riser to calculate its fatigue life challenging.

It has been demonstrated that increasing the installation angle used will increase the post-installation trench depth and moment envelopes of the riser both during installation. Also, when installation was taken into consideration, the additional trench formation due to operational loading was greatly reduced and the working load moments were increased. This informs the recommendation that this angle is kept to a minimum to reduce these moments.

Finally, a parametric study looking at the effect of the riser's diameter and penetration rate on trench depth and bending moments identified that increasing the riser's diameter had a detrimental effect on its fatigue life but increasing the penetration rate served to reduce the maximum moments experienced by it. Therefore it is sensible to try and keep the riser's diameter to a minimum.

Overall, installation has been shown to be one of the most critical loading scenarios during the life of a SCR and the development of the MATLAB model to simulate this has enabled more realistic bending moment and trench depth predictions which will allow for improved fatigue life estimates.

6 References

2H Offshore Engineering Ltd., 2006. *Installation of Risers in Deep Waters.* Kuala Lumpur, PetroMin Deepwater and Subsea Technology Conference and Exhibition.

Aubeny, C. & Biscontin, G., 2006. *Seafloor Interaction with Steel Catenary Risers,* Texas A&M University: Offshore Technology Reserach Center Report.

Aubeny, C. & Biscontin, G., 2009. Seafloor-Riser Interaction Model. *International Journal of Geomechanics,* pp. 133-141.

Aubeny, Shi & Murff, 2005. Collapse load for cylinder embedded in trench in cohesive soil. *Int. J. Geomech,* pp. 320-325.

Bhat, S., Jain, S., Randolph , M. & Mekha, B., 2013. *Modeling the touchdown zone trench and its impact on SCR fatigue life.* s.l., OTC 2013.

Bridge, C., 2005. *Effects of Seabed Interaction on Steel Catenary Risers,* s.l.: PhD Thesis, University of Surrey.

Bridge, C. et al., 2003. *Full scale model tests of a steel catenary riser,* s.l.: 2H Offshore Engineering Ltd.

Bridge, C. & Howels, H., 2007. *Observations and modeling of steel catenary riser trenches.* Lisbon, ISOPE-2007-468, pp. 803-813.

Bridge, C., Laver, K., Clukey, E. & Evans, T., 2004. *Steel catenary riser touchdown point vertical interaction model.* Houston, s.n.

Bridge, C. & Willis, N., 2002. *Steel Catenary Risers - Resuilts and Conclusions from Large Scale Simulations of Seabed Interaction.* s.l., 2hoffshore.com.

Callegari & Lenci, 2005. Simple analytical models for the J-lay problem. *Acta Mechanica,* Issue 178, pp. 23-39.

Clukey, E., Ghosh, R., Mokarala, P. & Dixon, M., 2007. *Steel Catenary Riser (SCR) design issues at touch down area.* Lisbon, Proceedings of the Seventeenth International Offshore and Polar Engineering Conference.

Clukey, E., Houstermans, L. & Dyvik , R., 2005. *Model tests to simulate riser-soil interaction effects in touchdown point region.* Perth, Australia, International Symposium on Frontiers in Offshore Geotechnics.

Dunlap, W. A., Bhojanala, R. P. & Morris, D. V., 1990. *Burial of Vertically loaded Offshore Pipelines in Weak Sediments.* Houston, Texas, s.n., pp. 263-270.

Giertsen, E., Verley, R. & Schroder, K., 2004. *CARISIMA a catenary riser/soil interaction model for global riser analysis.* Vancouver, Proceedings of the International Conference on Offshore Mechanics and Arctic Engineering.

Hale, J., Morris , D., Dunlap, W. & Yen , T., 1992. *Modeling pipeline behavior on clay soils during storms.* Houston, TX, 24th Offshore Technology Conference.

Hetenyi, M., 1946. *Beams on Elastic Foundation,* s.l.: The University of Michigan Press.

Howells, H., 1998. *Steel catenary risers for deepwater environments.* Houston, s.n., pp. 1-14.

Karunakaran, D., Farnes, K. A. & Giertsen, E., 2004. *Analysis guidelines and application of a riser-soil interaction model including trench effects.* Vancouver, Canada, Proceedings of the International Conference on Offshore Mechanis and Arctic Engineering.

Kim, K., Prezzi, M., Salgado, R. & Lee, W., 2008. Effect of Penetration Rate on Cone Penetration Resistance in Saturated Clayey Soils. *Journal of Geotechnical and Geoenvironmental Engineering,* pp. 1142-1153.

Mekha, B. B., 2001. New frontiers in the design of steel catenary risers for floating production systems. *Journal of Offshore Mechanics and Artic Engineering,* pp. 123, 153-158.

Morris, D., Webb, R. & Dunlap, W., 1988. *Self-burial of laterally loaded offshore pipelines.* Houston, Texas, 20th Annual Offshore Technology Conference.

Nakhaee, A. & Zhang, J., 2008. *Effects of the interaction with the seafloor on the fatigue life of a SCR.* Vancouver, International Offshore and Polar Engineering Conference.

Pesce, C., Aranha, J. & Martins, C., 1998. *The soil rigidity effect in the touchdown boundary layer of a catenary riser: static problem.* Montreal, Canada, Proceedings of the Eighth International Society of Offshore and Polar Engineers.

Pulici, Trifon & Dumitrescu, 2003. *Deep Water Sealines Installation by Using the J-lay Method - The Blue Stream Experience.* Honolulu, Thirteenth International Offshore and Polar Engineering Conference.

Yen, B. C., Allem, R. L. & Shatto, H. H., 1975. *Geotechnical Input for Deep-water Pipelines.* University of Delaware, ASCE, pp. 504-522.

You, J. H., 2012. *Numerical modeling of seafloor interaction with steel catenary risers,* Texas: Texas A & M University.

7 Appendices

7.1 Appendix 1: Risk assessment

When filling out the risk assessment form at the beginning of the year the only hazards identified related to this project were to do with computer use. This has proved to be true as the whole project has been solely computer based. In order to mitigate some of the risks good posture and ergonomics was used at all times and regular breaks were taken to prevent eye strain and stiff muscles.